

Preclinical validation and mechanistic understanding of drug repurposing candidates for polycystic kidney disease Kanhai. A.A.

Citation

Kanhai, A. A. (2025, October 28). *Preclinical validation and mechanistic understanding of drug repurposing candidates for polycystic kidney disease*. Retrieved from https://hdl.handle.net/1887/4280870

Version: Publisher's Version

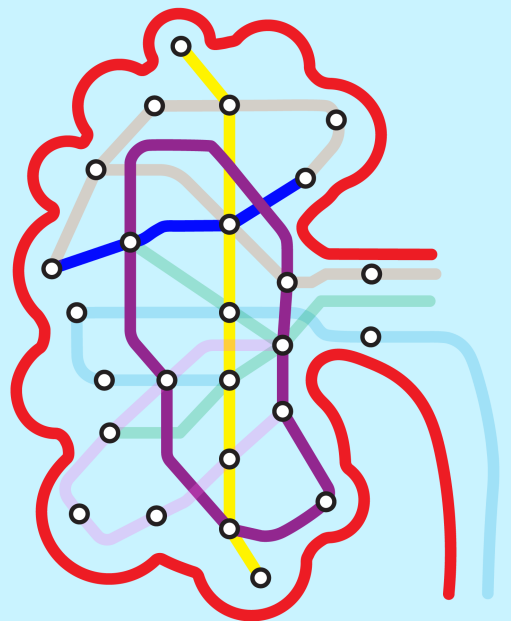
Licence agreement concerning inclusion of doctoral

License: thesis in the Institutional Repository of the University

of Leiden

Downloaded from: https://hdl.handle.net/1887/4280870

Note: To cite this publication please use the final published version (if applicable).



CHAPTER 3

Salsalate, but not metformin or canagliflozin, slows kidney cyst growth in an adult-onset mouse model of polycystic kidney disease

Wouter N. Leonhard^{1*}, Xuewen Song^{2*}, Anish A. Kanhai¹, Ioan-Andrei Iliuta², Andrea Bozovic³, Gregory R. Steinberg⁴, Dorien J.M. Peters^{1#}, York Pei^{2#}

¹Department of Human Genetics, Leiden University Medical Center, The Netherlands ²Division of Nephrology, University Health Network, Toronto, Ontario, Canada; Division of Nephrology, University of Toronto, Toronto, Ontario, Canada

³Laboratory Medicine and Pathobiology, University Health Network, Toronto, Ontario, Canada; Laboratory Medicine and Pathobiology, University of Toronto, Toronto, Ontario, Canada ⁴Centre for Metabolism, Obesity and Diabetes Research, McMaster University, Hamilton, Ontario, Canada ⁵Shared first author

*Shared senior author

EBioMedicine. 2019 Sep:47: 436-445

Abstract

Background: Multiple preclinical studies have highlighted AMP-activated protein kinase (AMPK) as a potential therapeutic target for autosomal dominant polycystic kidney disease (ADPKD). Both metformin and canagliflozin indirectly activate AMPK by inhibiting mitochondrial function, while salsalate is a direct AMPK activator. Metformin, canagliflozin and salsalate (a prodrug dimer of salicylate) are approved for clinical use with excellent safety profile. Although metformin treatment had been shown to attenuate experimental cystic kidney disease, there are concerns that therapeutic AMPK activation in human kidney might require a higher oral metformin dose than can be achieved clinically.

Methods: In this study, we tested metformin-based combination therapies for their additive (metformin plus canagliflozin) and synergistic (metformin plus salsalate) effects and each drug individually in an adult-onset conditional *Pkd1* knock-out mouse model (n = 20 male/group) using dosages expected to yield clinically relevant drug levels.

Findings: Compared to untreated mutant mice, treatment with salsalate or metformin plus salsalate improved kidney survival (i.e. blood urea nitrogen < 20 mmol/L at the time of sacrifice) and reduced cystic kidney disease severity. However, the effects of metformin plus salsalate did not differ from salsalate alone; and neither metformin nor canagliflozin was effective. Protein expression and phosphorylation analyses indicated that salsalate treatment was associated with reduction in mTOR (mammalian target of rapamycin) activity and cellular proliferation in *Pkd1* mutant mouse kidneys. Global gene expression analyses suggested that these effects were linked to restoration of mitochondrial function and suppression of inflammation and fibrosis.

Interpretation: Salsalate is a highly promising candidate for drug repurposing and clinical testing in ADPKD.

Introduction

Autosomal dominant polycystic kidney disease (ADPKD) is the most common inherited kidney disease worldwide with a life-time risk of at least 1/1000 in the general population¹. Mutations of two genes, *PKD1* and *PKD2*, account for 75–85% and 15–25% of the genetically resolved cases²⁻⁵. Disease progression of ADPKD is highly variable in part due to gene locus and allelic effects with the most severe disease associated with *PKD1* protein-truncating mutations, intermediate disease severity with *PKD1* non-truncating mutations, and mild disease with *PKD2* mutations³⁻⁵. Progressive increase in cyst number and size with age results in distortion of the normal kidney architecture and ultimately, end stage renal disease (ESRD) in a majority of patients⁶. Additionally, non-kidney related complications such as intracranial arterial aneurysms, polycystic liver, and heart valve defect also contribute to the morbidity and mortality of this disease⁷. Overall, ADPKD accounts for 5–10% of ESRD in the developed countries.

The pathobiology of ADPKD is not well understood but a "threshold model" of cystogenesis is supported by recent studies⁷⁻⁹. Under this model, variable reduction of cellular levels of functional polycystin-1 (i.e. the protein encoded by *PKD1*) due to germline and somatic mutations and stochastic factors, can influence cystic disease severity by modulating a complex array of signalling pathways⁸⁻¹⁰. However, restoration of functional polycystin-1 levels toward normal in cystic tissues presently remains an elusive therapeutic goal. By contrast, targeting key signalling pathways that drive cyst growth holds much promise for therapeutic development and clinical translation⁷. Indeed, the realization that increased cAMP signalling is a key driving mechanism for cyst growth and fluid secretion has led to the development of vasopressin V2 receptor (V2R) based therapy. Tolvaptan, an oral V2R antagonist which lowers [cAMP]i to slow cyst growth and delay loss of kidney function, has been recently approved as the first disease-modifier drug for treatment of ADPKD in multiple countries¹¹⁻¹⁵. However, tolvaptan is an expensive drug associated with significant side-effects, rendering its use restricted to high-risk patients. There is an urgent need for developing additional treatment for ADPKD.

Multiple experimental studies have highlighted the importance of mTORC1 (mammalian target of rapamycin complex 1) activation in modulating cyst growth in ADPKD¹⁶⁻²². Notably, therapeutic mTORC1 inhibition was highly effective in preclinical studies¹⁶⁻¹⁸. However, the results of two randomized controlled clinical trials of mTORC1 inhibitors in ADPKD demonstrated that low-dose treatment was ineffective²³ while high-dose treatment was associated with severe toxicities²⁴. An upstream inhibitor of the mTORC1 pathway is the AMP-activated protein kinase (AMPK). AMPK is a highly conserved and ubiquitously expressed heterotrimeric enzyme complex (consisting of α , β and γ isoforms) that functions as a sensor

of cellular energy status²⁵. By inhibiting mitochondrial function leading to reductions in the cellular adenylate charge and subsequent activation of the kinase through the interactions with the AMPK gamma isoforms, metformin, an inexpensive and generally safe anti-diabetic drug, activates AMPK indirectly²⁵⁻²⁷. Of interest, intra-peritoneal injections of metformin were found to attenuate cystic kidney disease in *Pkd1* mutant mice by activating AMPK and inhibiting mTORC1 signalling¹⁹. These promising results have led to the testing of metformin for ADPKD in a phase II clinical trial²⁸. However, reduced bioavailability (\sim 50–60%) and gastrointestinal intolerance (in \sim 30% of patients) coupled with a high hepatic first-pass effect (i.e. liver concentrating a high percentage of drug after gut absorption) raise concerns that the maximal oral dose of metformin (i.e. 2.0 g/day) used clinically may not be sufficient for therapeutic AMPK activation in the kidney^{29,30}. Thus, there is a need to develop more effective AMPK-based therapeutics which can be translated to treat patients with ADPKD.

In this study, we explored whether the addition of a second AMPK activating drug to metformin would enhance its therapeutic effects for experimental treatment of ADPKD. One of these drugs was a recently approved type 2 diabetic medication, canagliflozin, also an indirect AMPK activator like metformin^{31,32}. In addition, we also examined the effects of salsalate, a prodrug dimer of salicylate, which in contrast to metformin and canagliflozin, activates AMPK through direct interactions with the drug-binding domain of the AMPK $\beta 1$ isoform^{25,33}. Importantly, previous studies have indicated that given their distinct mechanisms for activating AMPK, there are synergies between metformin and salsalate therapy for treating fatty liver disease and suppressing mTOR in cancer cells^{34,35}. All three drugs have excellent safety profile and may be appropriate for drug repurposing to treat ADKPD³⁶.

To examine the additive (metformin plus canagliflozin) or synergistic (metformin plus salsalate) effect of metformin combination therapy, we tested in this study the efficacy of oral treatment of (i) metformin, (ii) canagliflozin, (iii) salsalate, (iv) metformin plus canagliflozin, (v) metformin plus salsalate vs. (vi) untreated mutant control in an adult-onset *Pkd1* conditional deletion mouse model.

Materials and methods

Mouse experimental protocol

The experimental design of our study is shown in Fig. 1. All the study groups were run concurrently in one large experiment. We used the iKsp-Pkd1^{del} conditional knock-out (KO) mice on a C57BL6/J congenic background for the testing^{10,37}. Twenty male mice/group were treated with tamoxifen (150 mg/kg, by oral gavage) at days P18 and P19 to inactivate Pkd1 which will lead to renal failure at around 4 months of age. Drug treatment began on day P40. Metformin (AK-Scientific, # I506) was administered orally in drinking water at 1.5 mg/mL (or ~ 300 mg/kg/day); canagliflozin (MedChemExpress, # HY-10451) was administered orally at 10 mg/kg/day (62.5mg/kg of food pellets (RM3(E)), Special Diet Services); and salsalate (AK-Scientific, #F817) was administered orally at 400 mg/kg/day (2.5 g/kg of food pellets, Special Diet Services). As control, one group of mice received food pellets generated by the same protocol, but without any drug. Blood urea nitrogen (BUN) was measured weekly starting at day P75 using 30 µl blood samples from the tail vein (Reflotron technology, Roche). All mice with a BUN >20 mmol/L were considered to have ESRD and sacrificed; BUN of WT mice was \sim 9 mmol/L. When \sim 50% of the untreated mice reached ESRD at 111–115 days of age, all mice from the control and other treatment groups were sacrificed within 5 days. For mice with BUN >20 mmol/L, the time to ESRD was calculated by linear interpolation of the ages between the last two BUN measurements. The age at ESRD or at censoring (i.e. mice without ESRD at the time of their last BUN measurement between 111 and 115 days of age) was used for Kaplan Meier survival analysis. All animal experiments were approved by the Animal Experiment Committee of the Leiden University Medical Centre and the Commission Biotechnology in Animals of the Dutch Ministry of Agriculture, and performed in accordance to Directive 2010/63/ EU for animal experiments.

Measurement of drug and cAMP levels

We measured serum metformin levels by an in-house assay we developed using liquid chromatography tandem mass spectrometry (LC-MS/MS) at the Clinical Biochemistry Laboratory of the Toronto General Hospital (see Supplementary Information). We measured serum salicylate levels using a commercially available kit (Neogen Corporation) and kidney tissue cAMP using the Direct cAMP ELISA kit (Enzo Life Sciences), according to the manufacturer instructions. Serum drug levels were measured in individual mutant mice after at least one month of treatment in the metformin group (n = 20) and salsalate group (n = 21) and at the time of sacrifice in the metformin group only (n = 19). Canagliflozin was not measured directly, but was expected to induce osmotic diuresis and hence, increased water intake was used as a surrogate marker of the drug effect. Indeed, we observed ~ 1.5 fold increased water intake in canagliflozin-treated mice.

Histological studies of kidney tissues

Kidneys were fixed in 4% buffered formaldehyde solution and embedded in paraffin. Periodic acid—Schiff (PAS) and Sirius Red staining was performed using standard protocols. F4/80 staining was used to detect macrophages. In brief, proteinase K antigen retrieval was used followed by a 20 min 0.12% H₂O₂ incubation step to block endogenous peroxidase. The sections were then incubated with rat anti-F4/80 (1:100; Serotec), followed by a second incubation step with anti-rat ImmPRESS™ (Vectorlabs). Immune reactions were revealed using diaminobenzidine as a chromogen and counterstained with hematoxylin, dehydrated, and mounted. Quantifications were done using Photoshop software as described previously³⁷. Colour palettes were designed to select pixels specific for those within cysts, those of the red Sirius Red signal (large arteries were excluded from the analyses), or those of the brown F4/80 signal. The total number of pixels from the entire section (without cysts) and the total number of pixels from either the Sirius red or F4/80 signal were used to calculate the percentage of Sirius Red or F4/80 staining within the entire kidney section.

Gene expression and bioinformatics analysis

Using the Mouse Gene 2.0 ST Arrays (Affymetrix), we performed global gene expression profiling of 30 kidney samples (wild-type, n = 7; KO mice, n = 12, and KO mice treated by salsalate, n = 11) which were selected around the median of the cystic index from each group. Microarray gene expression studies were performed by the Centre for Applied Genomics Core at the Hospital for Sick Children (Toronto, Ontario, Canada). QC measures and filtering are detailed in the Supplementary Information and in Figs. S1, S4, and S5. Differentially expressed genes were split into two groups of up-regulated and down-regulated genes. The lists of up-regulated and down-regulated genes were each used for gene set enrichment analysis (GSEA). We used Enrichr as the primary tool for GSEA³⁸. We used Benjamini-Hochberg (false discovery rate) FDR-adjusted p-values and Z-scores computed by Enrichr for the ranking of each gene set. Hierarchical clustering analysis and heatmap were performed using the DNA-Chip Analyzer (dChip) software package³⁹.

Western blot analysis

Protein extraction from whole kidney tissues for Western blot analysis are detailed in Supplementary Information. After collecting the supernatants from the kidney lysates, protein extracts were quantified using Protein Assay Kit (Bio-Rad) and then denatured in Laemmli sample buffer. Proteins were separated on TGX gradient gels (Bio-Rad) and then transferred onto PVDF membranes (Bio-Rad) by using Trans-Blot Turbo System (Bio-Rad). The membranes are incubated in blocking buffer (150 mM NaCl, 20 mM Tris, 5% skim milk, 0.1% Tween 20) for 60 min, and then incubated with primary antibodies at 4 °C overnight. Subsequently, primary antibody binding was detected with horseradish peroxidase (HRP)-conjugated anti-rabbit, or anti-mouse secondary antibodies, and proteins were visualized

with an enhanced chemiluminescence detection kit (ECL; Bio-Rad or Cell Signalling Technology). For determination of phospho/total protein levels, immunoblots were first probed for phospho levels, then stripped at RT for 30 min using Re-Blot Plus Mild Antibody Stripping Solution (EMD Millipore) and re-probed overnight to detect total levels. Protein expression was quantified by densitometric analysis with ImageJ software (NIH, http://rsbweb.nih.gov/ij/) according to the guidelines. All the primary and secondary antibodies used for this study are listed in Supplementary Information.

Quantification of mitochondrial DNA copy number

Total DNA containing mitochondrial and nuclear DNA (nDNA) was isolated by using QIAamp DNA Mini Kit (Qiagen). We performed quantitative real-time PCR using Power SYBR® Green PCR Master Mix (Applied Biosystems) with primers specific to a mitochondria-encoded gene, 16S ribosomal RNA (16s rRNA) (forward: 5'-CCGCAAGGGAAAGATGAAAGAC-3'; reverse: 5'-TCGTTTGGTTTCGGGGTTTC-3') and a nuclear-encoded gene, B2m (forward: 5'-GCCGAACATACTGAACTGCTAC-3'; reverse: 5'- GTGAGCCAGGATATAGAAAGACC-3'), as previously described⁴⁰. Mitochondrial DNA (mtDNA) copy number was estimated by the ratio of 16S rRNA/B2m.

Statistical analysis

Statistical analysis was performed using GraphPad Prism 7 software (San Diego, CA, USA). All results are expressed as dot-blots with median and interquartile ranges or mean ± SEM. Comparisons involving more than two groups were performed by one-way ANOVA followed by Tukey's or Dunnett's test post hoc; p-values corrected for multiple comparisons were reported. The Log Rank (Mantel-Cox) test was used for the Kaplan Meier survival analyses. The fibrotic index and F4/80 index between salsalate-treated and untreated *Pkd1* mice were tested using unpaired Student's t-tests.

Results

Salsalate, but not metformin or canagliflozin, slowed polycystic kidney disease

The iKsp-Pkd1^{del} mice were treated with clinically relevant drug doses according to experimental protocol (Fig. 1; also see Materials and Methods). When 46% of untreated Pkd1 mutant ('disease control') mice had reached ESRD by 111-115 days of age, all the mice from all study groups were sacrificed at that time. The mean serum metformin levels measured by LC-MS/MS in the mutant mice after at least one month of treatment (n = 20) and at the time of sacrifice (n = 19) were 14.6 (90% CI: 18.6-21.4) and 17.2 (90% CI: 14.1-20.3) uM, respectively. The median serum salicylate levels measured by ELISA in the mutant mice after at least one month of salsalate treatment (n = 21) was 222 (IQR: 108–372) µM. By comparison, the mean serum metformin and salicylate levels reported in diabetic patients on steady state clinical doses were 10 μmol/L and 1350 μmol/L, respectively^{29,30,41}. Moreover, in a pilot study of 5 PKD patients on 1.5-2 g/day of oral metformin, we found a median serum metformin level of 9.8 [range: 1.34 to 18.8] µmol/L (see Supplementary Information). These data indicate that clinically relevant serum drug levels were achieved in the metformin- and salsalate-treated mutant mice. Here we show that treatment with salsalate or metformin plus salsalate was associated with a significant improvement in kidney survival (Fig. 2a) and reduction in cystic kidney disease severity (Fig. 2b-d). However, the therapeutic effects of salsalate vs. metformin plus salsalate did not differ, suggesting that the therapeutic effects in the latter group was due to salsalate alone. Of note, the therapeutic effect of salsalate was very strong, and comparable to that by oral tolvaptan treatment using the same model and protocol in a separate study (manuscript in preparation). By contrast, treatment with metformin, canagliflozin, alone or together was not effective (Figs. 2, S2). A concern of metformin treatment is its potential for gastrointestinal side-effects including anorexia and

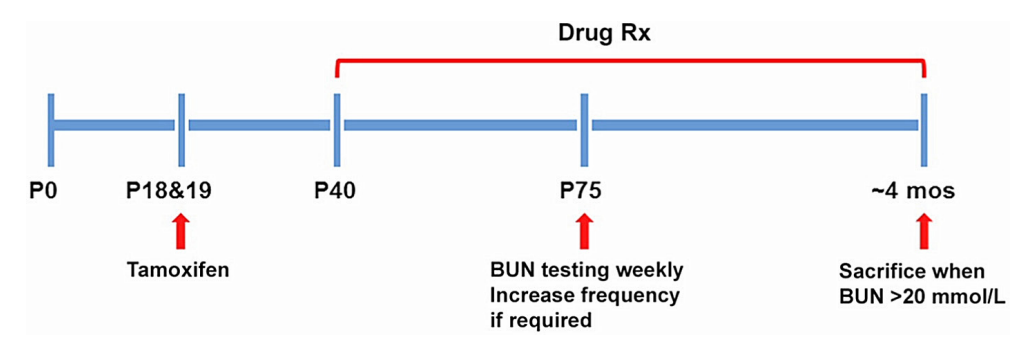


Figure 1. Experimental protocol

Twenty male iKsp- $Pkd1^{del}$ mice/group were treated with tamoxifen at days P18 and P19 to inactivate Pkd1 and drug treatment began on P40 (Rx). Untreated mutant mice began to develop advanced kidney failure at \sim P105. BUN monitoring via tail-vein blood sampling began at P75 to identify those mice with kidney failure; all mice with BUN > 20 mmol/L were considered to have ESRD and sacrificed. When \sim 50% of the untreated mutant mice reached ESRD, all the mice from all study groups were sacrificed.

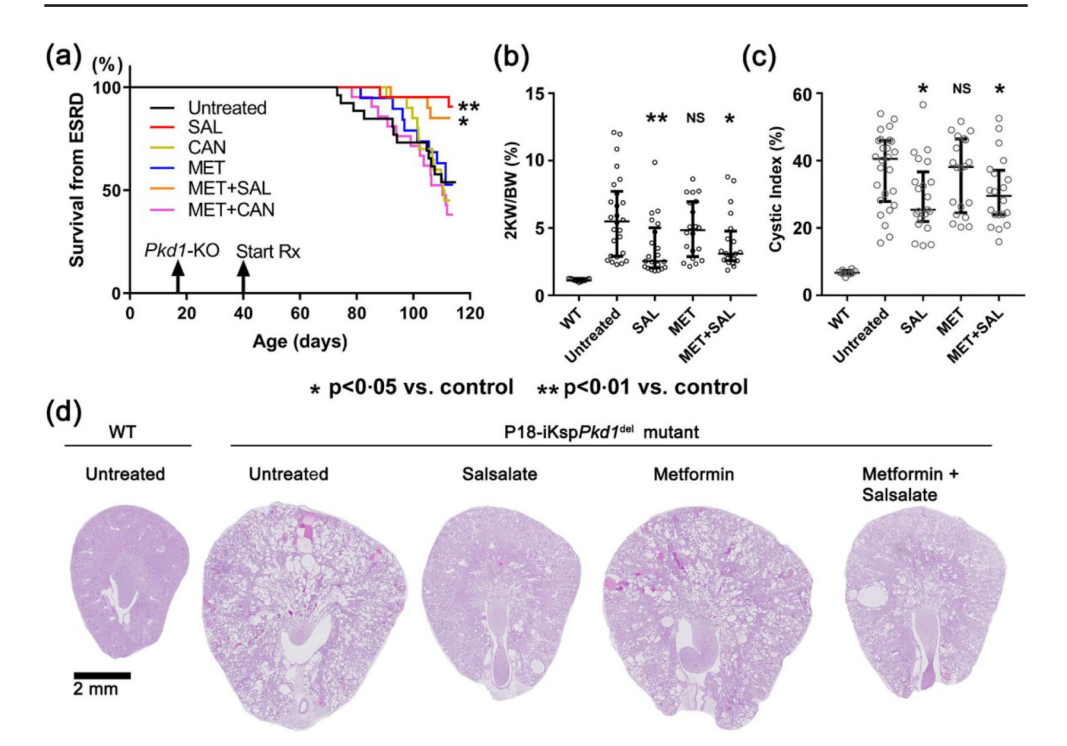


Figure 2: Salsalate treatment slowed progression of polycystic kidney disease in iKsp-Pkd1^{del} mice

(a) Only treatment with salsalate (SAL) or metformin plus salsalate (MET+SAL) was associated with a significant improvement in kidney survival. Only treatment with salsalate or metformin plus salsalate was associated with a significant reduction in (b) the ratio of two-kidney weight to body weight (2KW/BW) and (c) cystic index. There was no difference between treatment with MET+SAL and SAL suggesting the therapeutic effect of the former treatment group was likely due to salsalate alone. (d) Representative histological kidney sections (i.e. the median) from different study groups. NS denotes not significant. Data presented as mean \pm SEM; WT (n = 8), untreated (n = 26), SAL (n = 21), MET (n = 19), MET+SAL (n = 20).

diarrhea which can cause volume depletion. However, our metformin-treated mice appeared well and gained weight similar to mice from the other experimental groups throughout the study (Fig. S3). Moreover, there was an excellent correlation between BUN and 2KW/BW (Fig. S4) suggesting the loss of GFR was related to the cystic disease burden. Since treatment with metformin or canagliflozin was not effective, we focused our mechanistic study on salsalate.

Salsalate attenuated pathogenic mediators in Pkd1 mutant mouse kidneys

Aberrant mTORC1 activation¹⁶⁻²² and increased cAMP signalling^{7,11,13} in cystic tissues are two well-validated pathogenic mechanisms driving cyst growth in ADPKD. In turn, both of these pathogenic mechanisms have been shown to increase cystic epithelial cell proliferation while increased cAMP signalling also drives cystic fluid secretion¹¹. By Western blot analyses, we found that *Pkd1* mutant mouse kidneys (compared to wild type) displayed increased markers for mTORC1 activity (i.e. pS6K), cell proliferation (i.e. PCNA), and cell

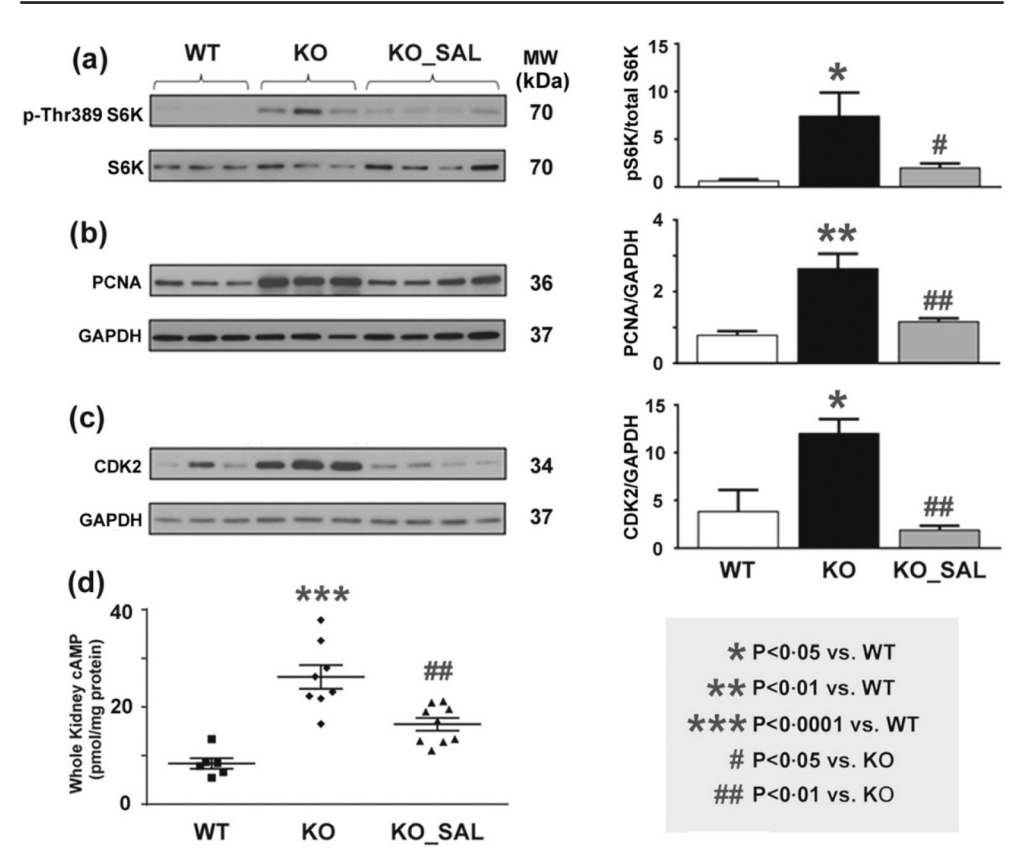


Figure 3: Salsalate reversed multiple pathogenic mediators of cystic kidney disease in iKsp-Pkd1^{del} mice

Western blot analyses showed that kidneys from mutant Pkd1 mice (compared to WT mice) displayed increased expression of protein markers for (a) mTORC1 activity (i.e. levels of pS6K), (b) cell proliferation (i.e. PCNA), (c) cell cycle progression (i.e. CDK2), and (d) cAMP; all these changes were significantly attenuated by salsalate treatment. Data presented as mean \pm SEM. For kidney cAMP levels, WT (n = 7), KO (n = 8), SAL (n = 9).

cycle progression (i.e. CDK2), as well as increased levels of cAMP; all of these changes were significantly attenuated by salsalate treatment (Fig. 3). However, we were unable to directly demonstrate increased AMPK activity which might be due to a number of technical issues (see Supplementary Information).

Salsalate treatment attenuated defective metabolism in Pkd1 mutant mouse kidneys

For a more comprehensive analysis of the molecular alterations, we performed gene expression profiling. Table 1 and Table 2 highlight the key findings. Of interest, the top 20 downregulated Reactome pathways and biological processes enriched in Pkd1 mutant mouse kidneys but attenuated by salsalate treatment were all related to metabolism. These results confirm our previous data indicating a generalized defect in metabolism in Pkd1 mutant kidneys with impaired fatty acid oxidation, amino acid catabolism and oxidative phosphorylation⁴², all these changes were attenuated by salsalate (Fig. 4a).

Table 1: Top ranked dysregulated Reactome pathways enriched in *Pkd1* mutant mouse kidneys but attenuated by salsalate treatment

| Т | | | | | |
|--|---|---------|--|-------|--|
| | Top down-regulated Reactome pathways enriched in iKsp- <i>Pkd1</i> ^{del} (vs. WT) mice | | Top up-regulated Reactom pathways in salsalate-treate (vs. untreated) iKsp- <i>Pkd1</i> ^{del} n | | |
| | Adjusted P-value* | Z-score | Adjusted P-value* Z-score | | |
| Metabolism | 6.49E-82 | -2.25 | 1.88E-69 | -2.25 | |
| The citric acid (TCA) cycle and respiratory electron transport | 6.94E-67 | -1.97 | 7.30E-50 | -1.97 | |
| Respiratory electron transport, ATP synthesis by chemiosmotic coupling, and heat production by uncoupling proteins | 1.12E-51 | -1.98 | 5.43E-38 | -1.98 | |
| Respiratory electron transport | 8.07E-46 | -1.95 | 1.15E-37 | -1.95 | |
| Complex I biogenesis | 3.61E-31 | -2.02 | 3.33E-23 | -2.02 | |
| Metabolism of lipids and lipoproteins | 1.12E-14 | -2.13 | 6.39E-22 | -2.19 | |
| Metabolism of amino acids and derivatives | 5.32E-14 | -2.15 | 2.12E-16 | -2.22 | |
| Pyruvate metabolism and Citric Acid (TCA) cycle | 1.21E-17 | -1.78 | 1.29E-13 | -1.81 | |
| Fatty acid, triacylglycerol, and ketone body metabolism | 1.16E-09 | -2.05 | 1.07E-12 | -2.17 | |
| Branched-chain amino acid catabolism | 1.24E-12 | -1.84 | 1.30E-10 | -2.03 | |
| Mitochondrial protein import | 3.73E-16 | -1.76 | 2.51E-09 | -1.76 | |
| Mitochondrial Fatty Acid Beta-Oxidation | 1.34E-09 | -1.40 | 5.04E-09 | -1.75 | |
| Citric acid cycle (TCA cycle) | 9.13E-13 | -1.84 | 3.08E-08 | -1.92 | |
| Metabolism of water-soluble vitamins and cofactors | 1.40E-15 | -1.88 | 3.08E-08 | -1.87 | |
| Peroxisomal lipid metabolism | 3.75E-14 | -1.99 | 3.68E-08 | -1.99 | |
| Glyoxylate metabolism and glycine degradation | 2.37E-11 | -1.54 | 1.38E-07 | -1.64 | |
| Histidine, lysine, phenylalanine, tyrosine, proline and tryptophan catabolism | 5.41E-12 | -1.66 | 3.56E-07 | -1.70 | |
| Mitochondrial translation | 3.82E-27 | -2.07 | 4.45E-07 | -1.96 | |
| Mitochondrial translation elongation | 1.75E-26 | -2.02 | 4.71E-07 | -1.91 | |
| Mitochondrial translation initiation | 1.92E-25 | -1.98 | 4.71E-07 | -1.88 | |

| Top 20 up-regulated Reactome pathways enriched in iKsp-Pkd1 del mouse kidneys but attenuated by salsalate treatment | | | | | |
|---|--|---|--|----------------|--|
| | Top up-regulated Reactome pathways enriched in iKsp-Pkd1 del (vs. WT) mice | | Top down-regulated Reactome pathways in salsalate-treated (vs. untreated) iKsp- <i>Pkd1</i> del mice | | |
| | Adjusted P-value* | Adjusted P-value* Z-score Adjusted P-value* | | | |
| Immune system | 1.01E-28 | -2.23 | 3.12E-35 | -2.23 | |
| Extracellular matrix organization | 6.10E-24 | -2.09 | 1.90E-33 | -2.10 | |
| Hemostasis | 1.44E-18 | -2.10 | 1.51E-23 | -2.13 | |
| Signalling by Rho GTPases | 1.42E-25 | -2.20 | 4.45E-22 | -2.18 | |
| Cytokine signalling in immune system | 2.67E-17 | -2.34 | 1.91E-17 | -2.37 | |
| Cell cycle, mitotic | 2.92E-23 | -2.44 | 3.04E-17 | -2.43 | |
| RHO GTPase effectors | 9.22E-19 | -2.23 | 8.48E-17 | -2.22 | |
| Axon guidance | 9.37E-14 | -2.28 | 8.95E-17 | -2.30 -2.39 | |
| Cell cycle | 1.99E-25 | -2.44 | 1.66E-16 | | |
| Developmental biology | 2.90E-12 | -2.27 | 1.77E-16 | -2.30 | |
| Innate immune system | 5.69E-15 | -2.36 | 2.16E-16 | -2.34 | |
| Integrin cell surface interactions | 6.19E-11 | -1.83 | 3.03E-15 | -1.89 | |
| Platelet activation, signalling and aggregation | 2.49E-12 | -2.06 | 5.11E-15 | -2.06 | |
| Cell-Cell communication | 1.02E-09 | -1.85 | 1.54E-13 | -1.92 | |
| Non-integrin membrane-ECM interactions | 8.67E-10 | -1.81 | 5.97E-13 | -1.89 | |
| Mitotic prometaphase | 2.91E-14 | -1.97 | 7.82E-12 | -1.92 | |
| RHO GTPases activate formins | 1.06E-12 | -1.94 | 1.92E-11 | -1.89 | |
| Interferon signalling | 4.27E-11 | -1.97 | 2.10E-11 | -1.96 | |
| Platelet degranulation | 3.35E-07 | -1.58 | 7.99E-11 | -1.77 | |
| Response to elevated platelet cytosolic Ca ²⁺ | 9.23E-11 | -1.75 | | | |

^{*}P-values computed by Fisher exact test and adjusted for multiple testing using the Benjamini-Hochberg method.

Table 2: Top ranked dysregulated biological processes enriched in *Pkd1* mutant mouse kidneys but attenuated by salsalate treatment

| Top 20 down-regulated biological processes enriched in iKsp-Pkd1 del mouse kidneys but attenuated by salsalate treatment | | | | | | |
|--|---|-------------------|---|-------|--|--|
| | Top down-regulated biological processes enriched in iKsp- <i>Pkd1</i> del (vs. WT) mice | | Top up-regulated biological processes in salsalate-treated (vs. untreated) iKsp-Pkd1 del mico | | | |
| | Adjusted P-value* | Adjusted P-value* | Z-score | | | |
| Respiratory electron transport chain | 6.90E-34 | -1.36 | 4.96E-28 | -1.36 | | |
| Mitochondrial ATP synthesis coupled electron transport | 3.35E-30 | -1.90 | 4.74E-25 | -1.90 | | |
| Fatty acid beta-oxidation | 2.82E-23 | -1.52 | 1.12E-21 | -1.53 | | |
| Fatty acid catabolic process | 4.99E-25 | -1.82 | 2.29E-19 | -1.83 | | |
| Mitochondrial respiratory chain complex assembly | 1.44E-29 | -1.78 | 2.29E-19 | -1.78 | | |
| Mitochondrial respiratory chain complex I biogenesis | 9.04E-27 | -1.58 | 8.73E-19 | -1.58 | | |
| NADH dehydrogenase complex assembly | 9.04E-27 | -1.57 | 8.73E-19 | -1.57 | | |
| Mitochondrial respiratory chain complex I assembly | 9.04E-27 | -1.41 | 8.73E-19 | -1.41 | | |
| Mitochondrial electron transport, NADH to ubiquinone | 2.54E-20 | -2.72 | 2.41E-18 | -2.72 | | |
| Fatty acid oxidation | 1.84E-19 | -1.81 | 1.08E-14 | -1.81 | | |
| Monocarboxylic acid metabolic process | 1.56E-11 | -1.64 | 7.54E-11 | -1.65 | | |
| Dicarboxylic acid metabolic process | 6.96E-12 | -1.82 | 1.31E-10 | -1.83 | | |
| Cellular respiration | 2.41E-15 | -1.24 | 4.59E-10 | -1.24 | | |
| Cellular amino acid catabolic process | 1.59E-11 | -1.68 | 7.19E-10 | -1.69 | | |
| Branched-chain amino acid catabolic process | 1.79E-11 | -1.77 | 2.53E-09 | -1.78 | | |
| Branched-chain amino acid metabolic process | 1.80E-09 | -1.74 | 5.34E-09 | -1.75 | | |
| Fatty acid metabolic process | 5.62E-10 | -1.31 | 5.34E-09 | -1.32 | | |
| Fatty acid beta-oxidation using acyl-CoA dehydrogenase | 4.92E-07 | -2.31 | 1.06E-07 | -2.32 | | |
| Coenzyme metabolic process | 8.55E-07 | -2.44 | 1.39E-07 | -2.48 | | |
| Mitochondrial transport | 4.26E-18 | -1.33 | 5.67E-07 | -1.33 | | |

| Top 20 up-regulated biological processes enriched in iKsp-Pkd1del mouse kidneys but attenuated by salsalate treatment | | | | | | |
|---|--|---------|---|-------|--|--|
| | Top up-regulated biological processes enriched in iKsp- <i>Pkd1</i> ^{del} (vs. WT) mice | | Top down-regulated biologi processes in salsalate-treat (vs. untreated) iKsp- <i>Pkd1</i> del I | | | |
| | Adjusted P-value* | Z-score | Adjusted P-value* Z-sc | | | |
| Extracellular matrix organization | 2.11E-27 | -1.65 | 1.76E-35 | -1.65 | | |
| Cellular response to cytokine stimulus | 5.98E-20 | -1.17 | 6.33E-23 | -1.17 | | |
| Regulation of cell migration | 1.98E-16 | -1.27 | 8.07E-22 | -1.27 | | |
| Cytokine-mediated signalling pathway | 1.05E-23 | -1.34 | 1.42E-21 | -1.34 | | |
| Neutrophil mediated immunity | 2.29E-08 | -1.90 | 1.11E-15 | -1.94 | | |
| Neutrophil degranulation | 4.15E-08 | -1.96 | 1.53E-15 | -2.01 | | |
| Response to cytokine | 1.22E-12 | -1.28 | 1.53E-15 | -1.28 | | |
| Neutrophil activation involved in immune response | 4.15E-08 | -1.23 | 2.61E-15 | -1.25 | | |
| Regulation of apoptotic process | 2.06E-11 | -1.77 | 1.26E-14 | -1.78 | | |
| Positive regulation of gene expression | 1.47E-13 | -1.66 | 2.87E-13 | -1.66 | | |
| Transmembrane receptor protein tyrosine kinase signalling pathway | 5.92E-14 | -1.74 | 1.75E-12 | -1.73 | | |
| Toll-like receptor signalling pathway | 2.55E-10 | -1.29 | 1.75E-12 | -1.29 | | |
| Regulation of cell proliferation | 6.56E-13 | -1.13 | 2.57E-12 | -1.12 | | |
| Protein phosphorylation | 1.50E-11 | -1.09 | 1.77E-11 | -1.09 | | |
| Positive regulation of transcription, DNA-templated | 8.62E-16 | -1.71 | 2.36E-11 | -1.69 | | |
| Cellular response to mechanical stimulus | 2.90E-10 | -2.15 | 3.14E-11 | -2.15 | | |
| Positive regulation of cell migration | 4.24E-08 | -1.87 | 3.14E-11 | -1.90 | | |
| Pattern recognition receptor signalling pathway | 1.17E-06 | -1.45 | 3.14E-11 | -1.47 | | |
| Platelet degranulation | 5.35E-06 | -1.38 | 3.14E-11 | -1.42 | | |
| Positive regulation of cell proliferation | 5.55E-09 | -1.54 | 3.96E-11 | -1.54 | | |

^{*}P-values computed by Fisher exact test and adjusted for multiple testing using the Benjamini-Hochberg method.

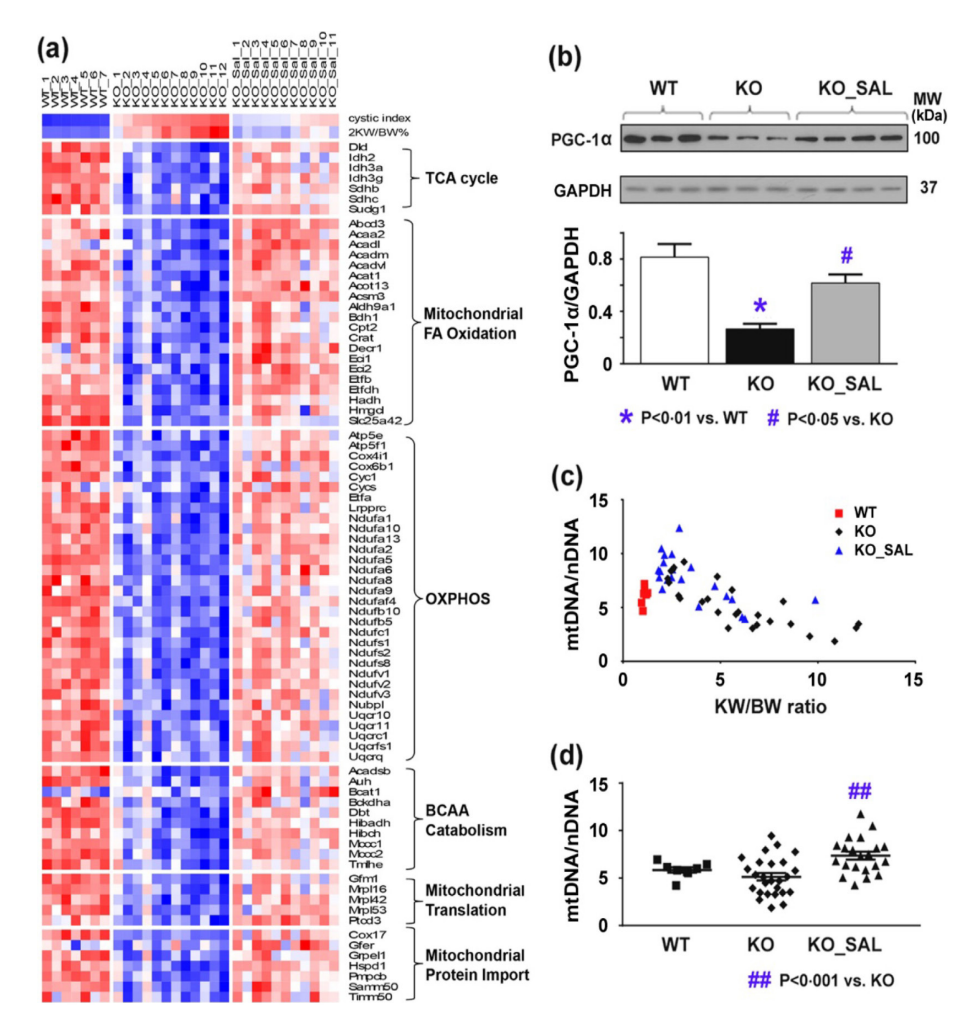


Figure 4: Salsalate treatment improved defective metabolism in Pkd1 mutant kidneys.

(a) Gene expression profiling showing changes consistent with a generalized defective metabolism with reduced oxidative phosphorylation (OXPHOS) and mitochondrial biogenesis in mutant (compared to WT) Pkd1 kidneys; these changes were attenuated by salsalate treatment (all changes shown were identified using a FDR adjusted p-value <0·01). Each column represents an individual kidney sample and each row represents the expression value of a specific gene; red indicates greater expression than the mean (white) value and blue, less than the mean value. (b) Western blot analysis confirming a decreased expression of PGC-1 α in Pkd1 mutant kidneys which was less pronounced by salsalate treatment. (c) An inverse correlation between mDNA/nDNA and KW/BW in Pkd1 mutant kidneys (r = -0·8, p < 0·0001) was noted consistent with defective mitochondrial biogenesis in ADPKD. (d) Salsalate treatment increased the ratio of mtDNA/nDNA in Pkd1 mutant kidneys. Data presented as mean \pm SEM. For kidney mtDNA qPCR, WT (n = 8), KO (n = 26), SAL (n = 21).

Reduced AMPK activity in cystic tissues is expected to decrease the activity of PGC-1 α , a master regulator for the transcriptional factors PPAR α , ERR α , and ERR γ ; all play a critical role in fatty acid oxidation and mitochondrial biogenesis⁴³. By Western blot analysis, we confirmed reduced PGC-1 α expression in *Pkd1* cystic kidneys, which was attenuated by salsalate (Fig. 4b). Our *in silico* analysis also predicted *Ppara* and its heterodimeric partner, *Rxr*, as the top-ranked transcriptional factors inhibited in *Pkd1* mutant kidneys, but active in the salsalate treatment group (Table S1). Consistent with defective mitochondrial biogenesis in ADPKD⁴⁴⁻⁴⁶, we found an inverse correlation between relative mitochondria copy number (using mtDNA/nDNA as a readout) and kidney weight/body weight in *Pkd1* cystic kidneys (r = -0.8, p < 0.0001) (Fig. 4c); the salsalate treated mice had higher mtDNA/nDNA ratios consistent with their milder PKD phenotype (Fig. 4d).

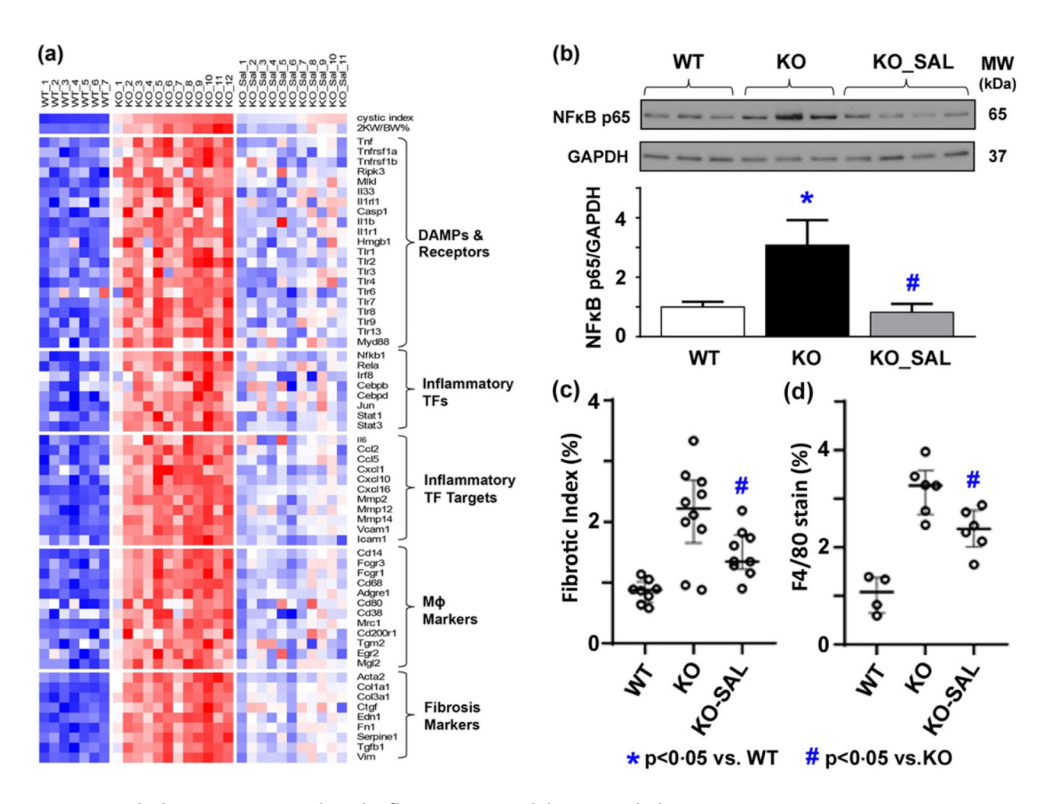


Figure 5: Salsalate treatment reduced inflammation in Pkd1 mutant kidneys.

(a) Gene expression profiling showing an increased expression of markers for damage-associated molecular patterns (DAMPs) and their receptors, macrophages (M Φ), inflammation and fibrosis in *Pkd1* mutant kidneys. Each column represents an individual kidney sample and each row represents the expression value of a specific gene; red indicates greater expression than the mean (white) value and blue, less than the mean value.(b) Western blot analysis showing an increased expression of NFkB p65 in *Pkd1* mutant kidneys. Histological analysis showing increased (c) fibrosis by Sirius Red staining and (d) macrophage infiltration by F4/80 staining in *Pkd1* mutant kidneys; all these changes were less severe by salsalate treatment. TF denotes transcriptional factor. Data presented as mean \pm SEM. For fibrotic index, WT (n = 8), KO (n = 10), SAL (n = 21); for F4/80 staining, WT (n = 4), KO (n = 6), SAL (n = 6).

Salsalate treatment attenuated inflammation in Pkd1 mutant mouse kidneys

Recent studies have documented that kidney tissue inflammation can promote progression of experimental ADPKD. Specifically, pharmacological and genetic manoeuvres depleting kidney tissue macrophage infiltration were shown to attenuate cystic disease severity^{47,48}. Interestingly, multiple top upregulated Reactome pathways and biological processes enriched in Pkd1 cystic kidneys but attenuated by salsalate were involved in immunity (Tables 1 and 2). By gene expression analysis, we found an increased expression of markers for damage-associated molecular patterns (DAMPs) and their receptors^{49,50}, macrophages, inflammation and fibrosis in Pkd1 cystic kidneys; all of these changes were attenuated by salsalate treatment (Fig. 5a). NFkB is a key regulator of innate immunity⁴⁹ and its p65 (Rela) subunit was predicted to be a top-ranked activated transcriptional factor in Pkd1 mutant kidneys, inhibited by salsalate (Table S1). We confirmed this finding by Western blot analysis (Fig. 5b). Consistent with our gene expression data, we found increased fibrosis and macrophage infiltration in Pkd1 mutant kidneys, which were attenuated by salsalate treatment (Figs. 5c, d and 6).

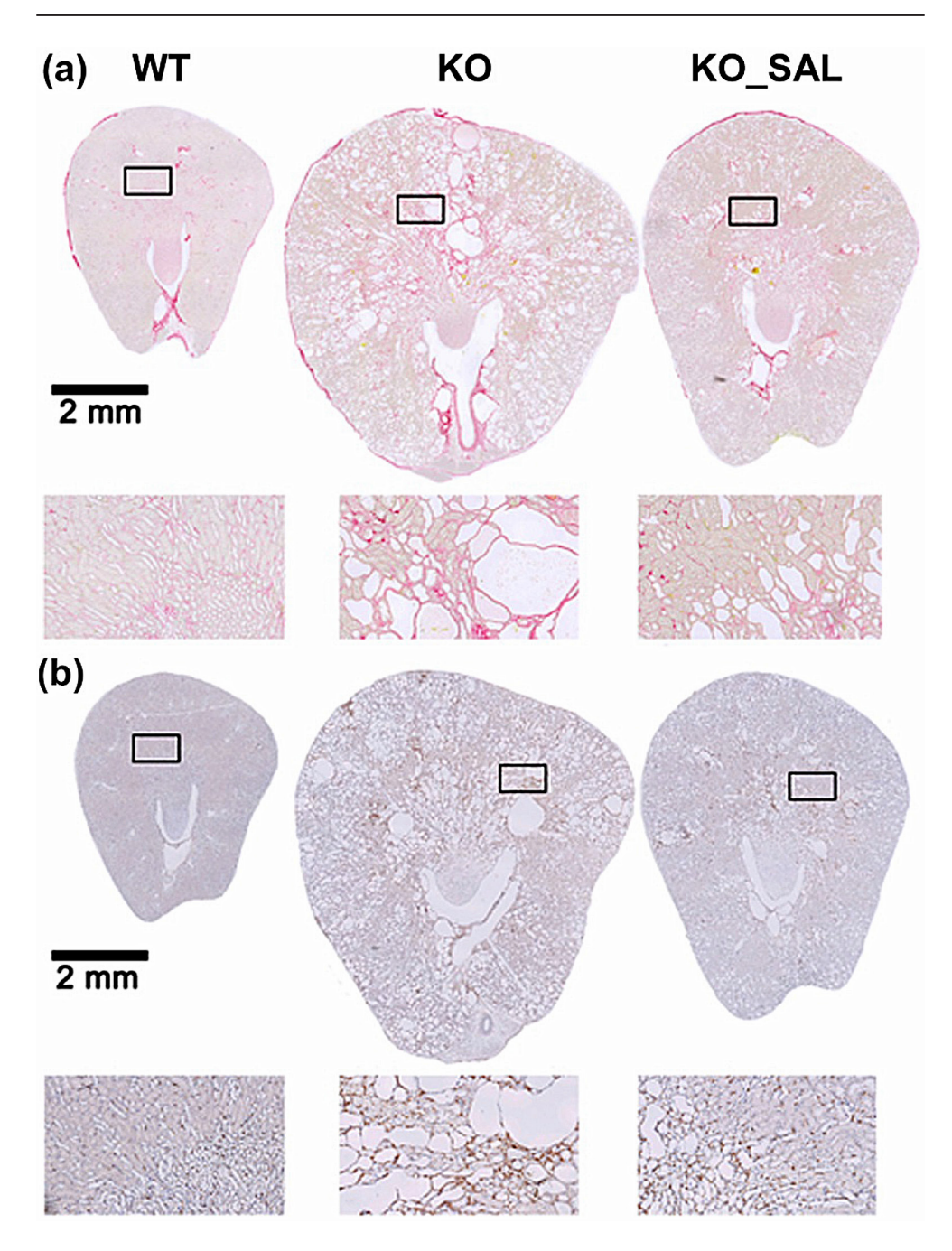


Figure 6: Salsalate treatment reduced fibrosis and inflammation in Pkd1 mutant kidneys.

Representative kidney sections showing (a) Sirius Red staining for collagen deposition as early marker for fibrosis and (b) F4/80 staining for macrophage infiltration. Salsalate treated *Pkd1* mutant (KO_SAL) mice had less fibrosis and macrophage infiltration compared to untreated *Pkd1* mutant (KO) mice.

Discussion

Given the concerns that therapeutic AMPK activation in the kidney might require a higher dose of oral metformin than can be achieved clinically^{26,27,29,30}, we tested metforminbased combination therapies for their additive (i.e. metformin plus canagliflozin) and synergistic (i.e. metformin plus salsalate) effects in an adult-onset Pkd1-deletion mouse model using dosages expected to yield clinically relevant drug levels²⁹⁻³³. We found that only salsalate (a prodrug dimer of salicylate) was effective in slowing PKD progression with serum salicylate levels at the lower clinical therapeutic range (i.e. 0.7-2.2 mmol/L)^{41,51}. By contrast, metformin was not effective despite serum drug levels in the clinical therapeutic range (i.e. 10 μmol/L)^{29,30}. Comparing our study to that by Takiar et al., which reported that intraperitoneal metformin treatment was effective in slowing PKD¹⁹, both studies used the same daily dose (i.e. 300 mg/kg). However, the bioavailability of oral metformin is only ~ 50%^{26,27}. More recently, oral metformin treatment was reported to slow PKD progression in a miniature pig model using a dose of 41.7 mg/kg/day⁵². However, the estimated human equivalent dose used for this study is 2.77 g/day, which is higher than the usual dose (2 g/ day) used clinically (see supplementary data)53. Differences in animal models and drug dosing in these studies may account for their discrepant results. However, serum metformin levels were not measured in these studies rendering them difficult to compare to our study. Preclinical studies that employ drug dosages modelling the clinical setting are more likely to have clinical relevance.

Increased mTORC1¹⁶⁻²⁰ and cAMP signalling¹¹⁻¹³ in cystic tissues are two major pathogenic mechanisms driving cyst growth in ADPKD. In turn, activation of these signalling pathways have been shown to increase cystic epithelial cell proliferation in virtually all models of PKD⁷ while increased cAMP signalling also drives cystic fluid secretion¹¹. In this context, our results are consistent with upregulation of these signalling pathways in the *Pkd1* mutant mouse kidneys which was attenuated by salsalate treatment. Our findings suggest that salsalate may have an additive therapeutic effect with tolvaptan by targeting cAMP signalling^{7,11-13}.

Recent studies have shown that Pkd1 cystic tissues display metabolic reprogramming consistent with a shift of the normal utilization of glucose through mitochondrial oxidative phosphorylation to aerobic glycolysis (a.k.a. the "Warburg effect") 20,21,54 . Instead of fully oxidizing one glucose molecule in the mitochondria to yield 36 ATP, cystic tissues prefer a metabolic pathway that generates only 4 ATP and 2 lactate molecules; the latter are then used to build macromolecules (nucleotides, proteins, lipids) to support cell proliferation 54 . In addition, defective fatty acid β -oxidation and altered mitochondrial function have been observed both *in vitro* and in animal models of ADPKD 44,55,56 . Indeed, the top 20

most downregulated gene pathways in Pkd1 mutant kidneys involved multiple metabolic processes ranging from tricarboxylic acid cycle, catabolism of fatty acids and amino acids, oxidative phosphorylation, to mitochondrial biogenesis; these changes suggest a generalized defective metabolism in Pkd1 mutant kidneys which was attenuated by salsalate treatment. Consistent with the findings by Lakhia et al.⁵⁷, our data suggest that decreased activity of PPAR α and PGC-1 α (co-activator of PPAR α) might contribute to the defective fatty acid oxidation and mitochondrial biogenesis in Pkd1 cystic tissues. Of interest, fenofibrate, a PPAR α agonist, was found in the former study to attenuate cystic kidney and liver disease in $Pkd1^{RC/RC}$ mice⁵⁷. However, the clinical use of this drug is limited by its potential nephrotoxicity, especially for patients with chronic kidney disease⁵⁸.

Tissue injury can initiate an inflammatory response through the actions of damage-associated molecule patterns (DAMPs) which comprise a heterogeneous group of molecules released during cell necrosis, tissue repair and remodelling. In turn, DAMPs can trigger innate immunity by activating Toll-like receptors, purogenic receptors, or NLRP3 inflammasome⁴⁹. Recent studies have shown that depletion of kidney macrophage infiltration by pharmacological and genetic manoeuvres attenuated *Pkd1* cystic disease severity^{47,48}. We found that *Pkd1* cystic kidneys were enriched with increased expression of genes encoding for multiple necrosis-related DAMPs, alarmins and their receptors (e.g. *Hmgb1* and *Tlr2/4*; *Tnf* and *Tnfrsf1a*; *Il33* and *Il1rl1*; *Il1b* and *Il1r1*) as well as pathway proteins (e.g. multiple toll-like receptors (TLRs), MyD88, NFkB; RIPK3 and MLKL) for innate immunity; all of these changes were attenuated by salsalate treatment⁵⁰. Taken together, our data are consistent with an emerging body of literature suggesting necroinflammation can provide an autoamplification loop of necrosis and inflammation that mediates progression of chronic kidney diseases⁵⁰. Thus, salsalate treatment may confer a therapeutic effect for other kidney diseases beyond ADPKD.

There are limitations or potential concerns in our study. First, our selection of samples closest to the median PKD severity for the gene expression studies might create bias by not including the outliers; nevertheless, this approach provides a valid assessment for the "average effect" of each study group. Second, metformin might result in volume depletion due to anorexia and diarrhea and a functional (i.e. renal vasoconstriction rather than structural damage) cause for increased BUN. However, our metformin-treated mice appeared well and gained weight similar to mice from other experimental groups throughout the study. There was also an excellent correlation between BUN and 2KW/BW which would not be expected if the rise of BUN was due to a functional cause. Nevertheless, there was a trend toward a steeper slope in the BUN vs. 2KW/BW correlation in the metformin-treated versus untreated mutant mice (Fig. S4), so a small functional effect on BUN could not be excluded. Lastly, since untreated mutant mice that reached ESRD were sacrificed earlier than the salsalate-treated

mutant mice, there is a bias in our study design to underestimate the salsalate treatment effects when 2KW/BW and cystic index were used as the outcome readouts.

In conclusion, using dosages expected to yield clinically relevant serum drug levels we found that salsalate, but not metformin or canagliflozin, was highly effective in attenuating renal cystic disease in an adult-onset Pkd1 mouse model. Of note, salsalate is a pro-drug which is released as two molecules of salicylate in the small intestine. Compared to aspirin (acetylsalicylic acid), salicylate displays weak cyclooxygenase enzyme inhibitory activities at clinical dose and is associated with minimal bleeding risk and fewer GI side-effects^{59,60}. Our observations of metabolic reprograming and inflammation in Pkd1 cystic kidneys (as compared to wild-type control) which were attenuated by salsalate treatment are consistent with the putative mechanisms of action of salicylate to directly activate AMPK³³, uncouple oxidative phosphorylation⁵¹, and strongly inhibit NF-κB⁵⁹. The oral bioavailability of salsalate in humans is \sim 80%; most of the salicylate is metabolized by the liver and excreted by the kidneys. With an excellent safety profile, salsalate, at concentrations capable of activating AMPK, has been used for over five decades for the treatment of arthritis and more recently re-purposed for testing in phase 2 clinical trials of type 2 diabetes and cardiovascular disease^{59,60}. These features, together with the results of our study, suggest that salsalate is a highly promising candidate for drug repurposing and clinical testing in ADPKD.

Author contributions

W.N.L., X.W.S., I.A.I., G.S., D.J.M.P., and Y.P. designed the study; W.N.L., X.W.S. and A.A.K. performed the study, analyzed the data, produced the figures and drafted the paper; A.B. developed the assays for and measured serum metformin levels; all the authors have read, edited and approved the final version of the manuscript.

Declaration of Competing Interest

Y.P. has served as consultant and received honoraria from Otsuka and Vertex Pharmaceutical. D.P. has served as consultant and received honorarium from Mironid. All other authors have nothing to disclose.

Acknowledgements

This work was supported in part by grants from the Canadian Institutes of Health Research (CIHR) Strategy for Patient Oriented Research (SPOR) program in Chronic Kidney Disease (CAN-SOLVE CKD SCA-145103), Polycystic Kidney Disease Foundation of Canada (to Y.P. and D.J.M.P.), and Dutch Kidney Foundation (NSN 15OKG01 to W.N.L. and 17PhD02 to

D.J.M.P. and W.N.L.). Some of the equipment used in this study was supported by the 3D (Diet, Digestive Tract and Disease) Centre funded by the Canadian Foundation for Innovation and Ontario Research Fund, project number 19442 and 30961.

References

- M.B. Lanktree, A. Haghighi, E. Guiard, et al. Prevalence estimates of polycystic kidney and liver disease by population sequencing. J Am Soc Nephrol, 29 (10) (2018), pp. 2593-2600
- D.J. Peters, L.A. Sandkuijl. Genetic heterogeneity of polycystic kidney disease in Europe. Contrib Nephrol, 97 (1992), pp. 128-139
- 3. Y.H. Hwang, J. Conklin, W. Chan, et al. Refining genotype-phenotype correlation in autosomal dominant polycystic kidney disease. J Am Soc Nephrol, 27 (6) (2016), pp. 1861-1868
- 4. E. Cornec-Le Gall, M.P. Audrézet, J.M. Chen, et al. Type of PKD1 mutation influences renal outcome in ADPKD. J Am Soc Nephrol, 24 (6) (2013), pp. 1006-1013.
- C.M. Heyer, J.L. Sundsbak, K.Z. Abebe, et al. Predicted mutation strength of nontruncating PKD1 mutations aids genotype-phenotype correlations in autosomal dominant polycystic kidney disease. J Am Soc Nephrol, 27 (9) (2016), pp. 2872-2884
- 6. J.J. Grantham, S. Mulamalla, K.I. Swenson-Fields. Why kidneys fail in autosomal dominant polycystic kidney disease. Nat Rev Nephrol, 7 (10) (2011), pp. 556-566
- P.C. Harris, V.E. Torres. Genetic mechanisms and signaling pathways in autosomal dominant polycystic kidney disease. J Clin Invest, 124 (6) (2014), pp. 2315-2324
- A.C. Ong, P.C. Harris. A polycystin-centric view of cyst formation and disease: the polycystins revisited. Kidney Int, 88 (4) (2015), pp. 699-710
- S.V. Fedeles, A.R. Gallagher, S. Somlo. Polycystin-1: a master regulator of intersecting cystic pathways. Trends Mol Med, 20 (5) (2014), pp. 251-260
- W.N. Leonhard, H. Happe, D.J. Peters. Variable cyst development in autosomal dominant polycystic kidney disease: the biologic context. J Am Soc Nephrol, 27 (12) (2016), pp. 3530-3538
- J.J. Grantham. Lillian Jean Kaplan international prize for advancement in the understanding of polycystic kidney disease. Understanding polycystic kidney disease: a systems biology approach. Kidney Int, 64 (4) (2003), pp. 1157-1162
- V.H. Gattone, X. Wang, P.C. Harris, V.E. Torres. Inhibition of renal cystic disease development and progression by a vasopressin V2 receptor antagonist. Nat Med, 9 (10) (2003), pp. 1323-1326
- V.E. Torres, X. Wang, Q. Qian, S. Somlo, P.C. Harris, V.H. Gattone. Effective treatment of an orthologous model of autosomal dominant polycystic kidney disease. Nat Med, 10 (4) (2004), pp. 363-364
- V.E. Torres, A.B. Chapman, O. Devuyst, et al. Tolvaptan in patients with autosomal dominant polycystic kidney disease. N Engl J Med, 367 (25) (2012), pp. 2407-2418
- V.E. Torres, A.B. Chapman, O. Devuyst, et al. Tolvaptan in later-stage autosomal dominant polycystic kidney disease. N Engl J Med, 377 (20) (2017), pp. 1930-1942

- J.M. Shillingford, N.S. Murcia, C.H. Larson, et al. The mTOR pathway is regulated by polycystin–1, and its inhibition reverses renal cystogenesis in polycystic kidney disease. Proc Natl Acad Sci U S A, 103 (14) (2006), pp. 5466-5471
- 17. J.M. Shillingford, K.B. Piontek, G.G. Germino, T. Weimbs. Rapamycin ameliorates PKD resulting from conditional inactivation of Pkd1. J Am Soc Nephrol, 21 (3) (2010), pp. 489-497
- Z. Novalic, A.M. van der Wal, W.N. Leonhard, et al. Dose-dependent effects of sirolimus on mTOR signaling and polycystic kidney disease. J Am Soc Nephrol, 23 (5) (2012), pp. 842-853
- V. Takiar, S. Nishio, P. Seo-Mayer, et al. Activating AMP-activated protein kinase (AMPK) slows renal cystogenesis. Proc Natl Acad Sci U S A, 108 (6) (2011), pp. 2462-2467
- I. Rowe, M. Chiaravalli, V. Mannella, et al. Defective glucose metabolism in polycystic kidney disease identifies a new therapeutic strategy. Nat Med. 19 (4) (2013), pp. 488-493
- M. Chiaravalli, I. Rowe, V. Mannella, et al. 2-deoxy-d-glucose ameliorates PKD progression. J Am Soc Nephrol, 27 (7) (2016), pp. 1958-1969
- G. Warner, K.Z. Hein, V. Nin, et al. Food restriction ameliorates the development of polycystic kidney disease. J Am Soc Nephrol, 27 (5) (2016), pp. 1437-1447
- A.L. Serra, D. Poster, A.D. Kistler, et al. Sirolimus and kidney growth in autosomal dominant polycystic kidney disease. N Engl J Med, 363 (9) (2010), pp. 820-829
- G. Walz, K. Budde, M. Mannaa, et al. Everolimus in patients with autosomal dominant polycystic kidney disease. N Engl J Med, 363 (9) (2010), pp. 830-840
- 25. G.R. Steinberg, D. Carling. AMP-activated protein kinase: the current landscape for drug development. Nat Rev Drug Discov, 18 (2019), pp. 527-551
- 26. I. Pernicova, M. Korbonits. Metformin--mode of action and clinical implications for diabetes and cancer. Nat Rev Endocrinol, 10 (3) (2014), pp. 143-156
- M. Foretz, B. Guigas, L. Bertrand, M. Pollak, B. Viollet. Metformin: from mechanisms of action to therapies. Cell Metab, 20 (6) (2014), pp. 953-966
- 28. S.L. Seliger, K.Z. Abebe, K.R. Hallows, et al. A randomized clinical trial of metformin to treat autosomal dominant polycystic kidney disease. Am J Nephrol, 47 (5) (2018), pp. 352-360
- 29. L. He, F.E. Wondisford Metformin action: concentrations matter. Cell Metab, 21 (2) (2015), pp. 159-162
- 30. N.S. Chandel, D. Avizonis, C.R. Reczek, et al. Are metformin doses used in murine cancer models clinically relevant? Cell Metab, 23 (4) (2016), pp. 569-570
- S.A. Hawley, R.J. Ford, B.K. Smith, et al. The Na+/glucose cotransporter inhibitor canagliflozin activates AMPK by inhibiting mitochondrial function and increasing cellular AMP levels. Diabetes, 65 (9) (2016), pp. 2784-2794
- L.A. Villani, B.K. Smith, K. Marcinko, et al. The diabetes medication Canagliflozin reduces cancer cell proliferation by inhibiting mitochondrial complex-I supported respiration. Mol Metab, 5 (10) (2016), pp. 1048-1056
- S.A. Hawley, M.D. Fullerton, F.A. Ross, et al. The ancient drug salicylate directly activates AMP-activated protein kinase. Science, 336 (6083) (2012), pp. 918-922
- R.J. Ford, M.D. Fullerton, S.L. Pinkosky, et al. Metformin and salicylate synergistically activate liver AMPK, inhibit lipogenesis and improve insulin sensitivity. Biochem J, 468 (1) (2015), pp. 125-132

- 35. A.J. O'Brien, L.A. Villani, L.A. Broadfield, et al. Salicylate activates AMPK and synergizes with metformin to reduce the survival of prostate and lung cancer cells ex vivo through inhibition of de novo lipogenesis. Biochem J, 469 (2) (2015), pp. 177-187
- 36. V. Padovano, C. Podrini, A. Boletta, M.J. Caplan. Metabolism and mitochondria in polycystic kidney disease research and therapy. Nat Rev Nephrol, 14 (11) (2018), pp. 678-687
- W.N. Leonhard, S.J. Kunnen, A.J. Plugge, et al. Inhibition of activin signaling slows progression of polycystic kidney disease. J Am Soc Nephrol, 27 (12) (2016), pp. 3589-3599
- M.V. Kuleshov, M.R. Jones, A.D. Rouillard, et al. Enrichr: a comprehensive gene set enrichment analysis web server 2016 update. Nucleic Acids Res, 44 (W1) (2016), pp. W90-W97
- 39. C. Li, W. Hung Wong. Model-based analysis of oligonucleotide arrays: model validation, design issues and standard error application. Genome Biol, 2 (8) (2001)
- P.M. Quiros, A. Goyal, P. Jha, J. Auwerx. Analysis of mtDNA/nDNA ratio in mice. Curr Protoc Mouse Biol, 7 (1) (2017), pp. 47-54
- 41. A. Fleischman, S.E. Shoelson, R. Bernier, A.B. Goldfine. Salsalate improves glycemia and inflammatory parameters in obese young adults. Diabetes Care, 31 (2) (2008), pp. 289-294
- T.B. Malas, C. Formica, W.N. Leonhard, et al. Meta-analysis of polycystic kidney disease expression profiles defines strong involvement of injury repair processes. Am J Physiol Renal Physiol, 312 (4) (2017), pp. F806-F817
- W. Fan, R. Evans. PPARs and ERRs: molecular mediators of mitochondrial metabolism. Curr Opin Cell Biol, 33 (2015), pp. 49-54
- V. Padovano, I.Y. Kuo, L.K. Stavola, et al. The polycystins are modulated by cellular oxygen-sensing pathways and regulate mitochondrial function. Mol Biol Cell, 28 (2) (2017), pp. 261-269
- 45. Y. Ishimoto, R. Inagi, D. Yoshihara, et al. Mitochondrial abnormality facilitates cyst formation in autosomal dominant polycystic kidney disease. Mol Cell Biol, 37 (2017), pp. e00337-e00417
- S. Hajarnis, R. Lakhia, M. Yheskel, et al. microRNA-17 family promotes polycystic kidney disease progression through modulation of mitochondrial metabolism. Nat Commun, 8 (2017), Article 14395
- 47. A. Karihaloo, F. Koraishy, S.C. Huen, et al. Macrophages promote cyst growth in polycystic kidney disease. J Am Soc Nephrol, 22 (10) (2011), pp. 1809-1814
- L. Chen, X. Zhou, L.X. Fan, et al. Macrophage migration inhibitory factor promotes cyst growth in polycystic kidney disease. J Clin Invest, 125 (6) (2015), pp. 2399-2412
- H.J. Anders, L. Schaefer. Beyond tissue injury-damage-associated molecular patterns, toll-like receptors, and inflammasomes also drive regeneration and fibrosis. J Am Soc Nephrol, 25 (7) (2014), pp. 1387-1400
- 50. S.R. Mulay, A. Linkermann, H.J. Anders. Necroinflammation in kidney disease. J Am Soc Nephrol, 27 (1) (2016), pp. 27-39
- 51. B.K. Smith, R.J. Ford, E.M. Desjardins, et al. Salsalate (salicylate) uncouples mitochondria, improves glucose homeostasis, and reduces liver lipids independent of AMPK-β1. Diabetes, 65 (11) (2016), pp. 3352-3361
- 52. X. Lian, X. Wu, Z. Li, et al. The combination of metformin and 2-deoxyglucose significantly inhibits cyst formation in miniature pigs with polycystic kidney disease. Br J Pharmacol, 176 (5) (2019), pp. 711-724

- 53. U.S. Department of Health and Human Services, Food and Drug Administration Center for drug evaluation and research. Guidance for industry: Estimating the maximum safe starting dose in initial clinical trials for the
- 54. M.G. Vander Heiden, L.C. Cantley, C.B. Thompson. Understanding the Warburg effect: the metabolic requirements of cell proliferation. Science, 324 (5930) (2009), pp. 1029-1033
- 55. L.F. Menezes, C.C. Lin, F. Zhou, G.G. Germino. Fatty acid oxidation is impaired in an orthologous mouse model of autosomal dominant polycystic kidney disease. EBioMedicine, 5 (2016), pp. 183-192
- 56. C.C. Lin, M. Kurashige, Y. Liu, et al. A cleavage product of Polycystin-1 is a mitochondrial matrix protein that affects mitochondria morphology and function when heterologously expressed. Sci Rep, 8 (1) (2018), p. 2743
- 57. R. Lakhia, M. Yheskel, A. Flaten, E.B. Quittner-Strom, W.L. Holland, V. Patel. PPARalpha agonist fenofibrate enhances fatty acid beta-oxidation and attenuates polycystic kidney and liver disease in mice. Am J Physiol Renal Physiol, 314 (1) (2018), pp. F122-F131
- 58. R.L. Attridge, C.R. Frei, L. Ryan, J. Koeller, W.D. Linn. Fenofibrate-associated nephrotoxicity: a review of current evidence. Am J Health Syst Pharm, 70 (14) (2013), pp. 1219-1225
- K. Anderson, L. Wherle, M. Park, K. Nelson, L. Nguyen. Salsalate, an old, inexpensive drug with potential new indications: a review of the evidence from 3 recent studies. Am Health Drug Benefits, 7 (4) (2014), pp. 231-235
- 60. G.R. Steinberg, M. Dandapani, D.G. Hardie. AMPK: mediating the metabolic effects of salicylate-based drugs? Trends Endocrinol Metab, 24 (10) (2013), pp. 481-487

Supplementary Methods

Mouse Studies

We used the inducible iKsp-Pkd1^{del} mice (tam-KspCad-CreER^{T2};Pkd1^{del2-11/lox2-11})¹ engineered with a kidney-specific tamoxifen-inducible Cre and two LoxP sites that flank exons 2-11 for the drug testing. These mice were bred into a C57BL6/J congenic background and the model (i.e. timing and dose of tamoxifen induction and disease severity) has been well characterized to provide a moderately aggressive disease course. Because of a gender dimorphism with male mice displaying more severe disease, we only studied the male mice to minimize disease variability. Metformin was administered orally in drinking water at 1.5 mg/ml (or ~ 300 mg/kg/day) and was expected to yield a serum level of ~ 5 -10 μ mol/L; similar to that seen in patients treated with the usual clinical dose (i.e. 1.5-2.5 g/day)^{2,3}. Canagliflozin was administered orally at 10 mg/kg/day in food pellets and was expected to produce a serum drug level area under the curve (AUC) measure of ~30 µgxh/ml; similar to that seen in patients treated with the maximal clinical dose (i.e. 300 mg/day; https://www. tga.gov.au/auspar/auspar-canagliflozin-hemihydrate-0). Salsalate was administered orally at 400 mg/kg/day in food pellets and was expected to produce a serum salicylate level of ~ 1 mmol/L; similar to that seen in patients treated with the clinical dose of 3-4 g/day^{4,5}. In a pilot study we had noted that canagliflozin-treated mice drank on average 1.5-2x more water than mice from the other groups due to their glycosuria. To avoid excess metformin dosing in mice treated with both canagliflozin and metformin, we measured weekly total water intake in these mice and applied a correction factor (i.e. x 0.5-0.7) to lower their metformin concentration in the drinking water.

Tissue Processing for DNA/RNA/Protein Studies

For the DNA/RNA/protein studies, we selected wild-type or mutant kidneys from each study group that clustered around the median of their cystic index. Half of each kidney was snap-frozen in liquid nitrogen, fragmented into powder in liquid nitrogen by BioPulverizer (BioSpec), and stored in a -80°C freezer for the above studies.

Microarray Gene Expression Analyses

Total RNA was extracted using miRNeasy Mini Kit (Qiagen) with an on-column DNA digestion step to minimize genomic DNA contamination. The sample integrity of the RNA was assessed using the RNA 6000 Nano Assay on 2100 Bioanalyzer (Agilent Technologies) to ensure that RNA integrity number (RIN) was greater than 9. In brief, 300 ng of total RNA was labelled using the GeneChip WT PLUS Reagent Kit (Affymetrix). Following fragmentation, 5·5 μg of biotin-labelled ss-cDNAs were then hybridized to GeneChip Mouse Gene 2.0 ST Arrays for 16 hours at 45°C. Hybridized arrays were then stained and washed in the Affymetrix Fluidics Station 450. Thereafter, the arrays were scanned on an Affymetrix GeneChip Scanner 3000 and the image (.DAT) files were preprocessed using the Affymetrix GeneChip Command Console (AGCC) software to generate cell intensity (.CEL) files. The latter files were then uploaded to the Transcriptome Analysis Console (TAC) 4.0 (Thermo Fisher Scientific) for further processing and quality control. The probe set signal intensities were then extracted and normalized using the robust multi-array average (RMA) algorithm embedded in TAC 4.0 software. Microarray data are MIAME compliant and available in Gene Expression Omnibus (GEO, http://www.ncbi.nlm.nih.gov/geo/; ID: GSE126454). Differentially expressed gene (DEG) probes affected by the genotype and treatment were determined by the Limma Bioconductor package implemented in TAC 4.0 using false discovery rate (FDR) < 5%. To get a list of genes for gene set enrichment analysis (GSEA), we applied a few filtering steps by eliminating redundant gene probes and filtering out probes without gene symbols and the genes with very low expression levels (mean expression values across all samples \leq 30, i.e. log2 transformed expression values ≤ 4.91). We used Enrichr as the primary tool for GSEA [6]. Enrichr currently contains a large collection of diverse gene set libraries (134 geneset libraries as of 2018) available for analysis. In this study we used the following gene-set libraries for GSEA: Reactome 2016 (database of biological pathways, n=1530) for signalling/ metabolic canonical pathways; GO_Biological_Process_2018 (n=5103) for biological processes; ChEA 2016 (ChIP-seq/chip enrichment analysis, n=645) for transcription factors (TFs); KEA 2015 (kinase-substrate database for kinase enrichment analysis, n=428) for kinases; and Phosphatase_Substrates_from_DEPOD (The human DEPhOsphorylation database, n=59) for phosphatases. As the enrichment analysis is sensitive to input genes of variable lengths, up- and down-regulated gene lists, the combined list, lists of different lengths ranked by their FDR p-values (top 100, 500, 1000, 2000) were also used as separate input lists for TF, kinase and phosphatase analysis, the top-ranked enriched data with higher overlap in these lists were identified as the key regulatory factors. An overview of the systems biology analysis is outlined in Figure S1. Table S1 shows a list of top-ranked inhibited and activated transcriptional factors enriched in *Pkd1* KO mouse kidneys reversed by salsalate treatment as predicted by Enrichr.

Western Blot Analysis

Kidney tissue samples were homogenized in 4°C lysis buffer containing 50 mM HEPES pH 7.4, 150 mM NaCl, 100 mM NaF, 10 mM Na pyrophosphate, 5 mM EDTA, 250 mM sucrose, 1 mM DTT, and 1 mM Na-orthovanadate, 1% Triton X, 0·2% SDS and Complete protease inhibitor cocktail (Roche)⁷. The lysates were incubated for 30 min. at 4°C and then centrifuged for 15 min. at 13000 rpm at 4°C. The primary antibodies for S6K1 (Cat #9202), pS6K1 Thr389 (Cat #9234), NFkB p65 (Cat #8242), PCNA (Cat #2586), GAPDH (Cat #5174) were obtained from Cell Signalling Technology and the antibodies for PGC-1 α (Cat #sc-517380) and CDK2 (Cat #sc-6248) were from Santa Cruz Biotechnology. The secondary antibodies for horseradish peroxidase (HRP)-conjugated anti-rabbit antibody (Cat #7074) and HRP-conjugated anti-mouse antibody (Cat #7076) were obtained from Cell Signalling Technology.

Estimating Human Equivalent Dose from Miniature Pig study of Metformin in ADPKD

Lian X-Y, et al. reported that metformin treatment was effective in slowing PKD in a miniature pig model using a dose of 41.7 mg/kg^8 . To estimate the Human Equivalent dose from the miniature pig study, we used the following parameters for the calculation according to the FDA guidelines for inter-species drug studies⁹.

Drug dose (mini-pig) = 41.7 mg/kg/day; Km (adult human) = 37; Km (mini-pig) = 35 Human Equivalent Dose = 41.7 mg/kg/day x 35/37 = 39.5 mg/kg/day or 2.77 g/day for a 70 kg person

Quantitation of Metformin in Mouse and Human Serum Samples using Liquid Chromatography-Tandem Mass Spectrometry

The aim of the work described here was to develop a liquid chromatography-tandem mass spectrometry-based assay (LC-MS/MS) for quantitation of metformin in mouse and human serum samples. **Chemicals:** Metformin HCl in methanol, primary standard was obtained from Sigma (St. Louis, MO). Isotopically labelled form, metformin-D6 hydrochloride was purchased from Toronto Research Chemicals (North York, Canada). Structures of the light

and heavy forms are shown in Fig. 1. Ultra-pure water was obtained from an in-house bench-top purification system ELGA PureLab (High Wycombe, UK). Methanol was Optima grade and was purchased from Fisher Scientific (Fair Lawn, NJ). Ammonium acetate was obtained from Sigma (Oakville, Canada). Optima-grade acetonitrile was purchased from Fisher Scientific (Fair Lawn, NJ).

Figure 1. Structures of metformin hydrochloride and metformin-D6 hydrochloride

LC-MS/MS instrument and conditions: Agilent 1200 series system (Agilent Technologies, US) consisting of a degasser, solvent binary pump, autosampler, chiller and a column oven was used for the study. The mobile phase consisted of 10 mM ammonium acetate (60%) and acetonitrile (40%). Separation was achieved on a reversed phase Kinetex Biphenyl, 100 x 3.0 mm, 2.6 μ m analytical column with an isocratic elution. The flow rate was kept at 500 μ l/min and an injection volume of 1 μ l was used. Column was maintained at 30 °C and the total analysis time was 3.0 minutes.

The LC system was coupled to an API 5000 triple quadrupole mass spectrometer (Applied Biosystems/MDS Sciex, Concord, ON, Canada) equipped with an electrospray ionization (ESI) probe. For quantitation the mass spectrometer was operated in the multiple reaction monitoring (MRM) and positive ion modes. The spray voltage was 5500 V and the capillary temperature was set at 600°C. The ion source gases: curtain gas, GS1 and GS2 were 30, 20, and 50, respectively. Nitrogen was collision gas with the value set at 4 U. The declustering potential (DP), collision energy (CE), and cell exit potential (CXP) were optimized for each transition and were as follows: 120, 19, 26 V for metformin (quantifier), 120, 28, 28 V for metformin (qualifier), and 143, 21, 24 V for internal standard. We monitored selective ion-transitions for both the light and heavy analyte: m/z 130.0>60.0 (quantifier) and m/z130.0>71.0 (qualifier) for metformin and m/z 136.0>60.0 for the internal standard. Dwell time per transition was 100 ms. The LC system and mass spectrometer were controlled by the Analyst software (version 1.6.2). Data acquisition and analysis were completed using the same software. Metformin concentrations were normalized by the response of the internal standard and quantified using the calibration curves that were included in each batch. Quality controls were used to ensure the accuracy of the measurements.

Preparation of standards and quality controls: Calibration standards (0.05, 0.1, 0.5, 1, 5, 10, 50 μ mol/I) were prepared by spiking pooled untreated mouse serum with appropriate amount of the working standard solution containing metformin. Stock solution of the internal standard (IS), 5.82 mmol/I was made by dissolving the pure compound in methanol. Working IS solution (500 nmol/I) was made in acetonitrile. The Quality control (QC) samples were prepared at two levels by adding metformin to untreated mouse serum. Calibration standards and quality control material were stored at -20°C.

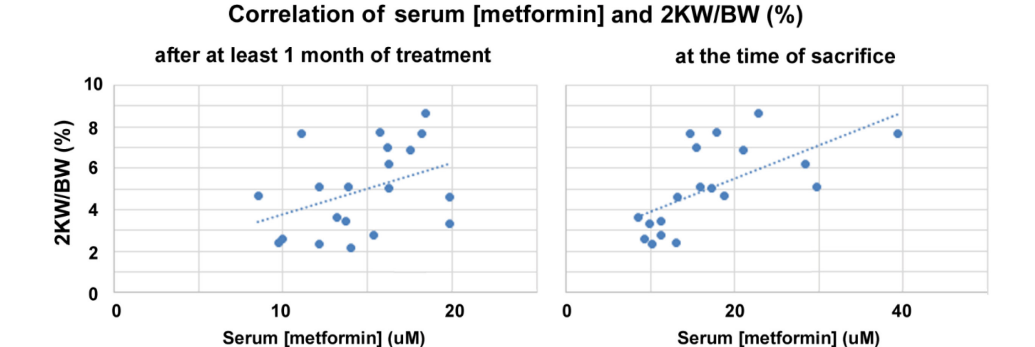
Sample preparation: The frozen serum samples (calibration standards, QC, treated mouse and human specimens) were allowed to thaw and equilibrate at room temperature prior to processing. Sample was vortexed for 5 s prior to transferring 10 μ l into a 1.5 ml microcentrifuge tube. 100 μ l of acetonitrile containing internal standard (500 nmol/l) was added to each tube using an electronic dispenser. After vortex-mixing for 30 s the samples were centrifuged for 10 min at 14,000 rpm. The supernatant was evaporated to dryness under N2 stream at 40°C. Sample was reconstituted in 100 μ l of solvent A and transferred into an autosampler vial or 96-well plate.

Validation

Linearity: Linearity of the method was assessed by analyzing calibration standards on multiple days. The calibration curves for both metformin transitions were linear between 0.05 and $50 \mu mol/l$ with correlation coefficient, $r \ge 0.9864$ for a total of 6 replicates accumulated over four days. The r values, slopes and intercepts were calculated using weighted (1/x) linear regression.

Precision: In order to assess within-day and between-day precision QC samples at low and middle concentrations were prepared as described above. The within-day precision was determined by calculating % CV for the five QC replicates analyzed on the same day. QC level 1 had a mean value of 0.06 μ mol/l with precision of 7.2%, while the mean for QC level 2 was 0.73 μ mol/l with precision of 6.1%. The between-day precision for the assay was assessed by analyzing eleven QC replicates over three days. Between-day precision at the QC level 1 (mean value 0.07 μ mol/l) was 8.0%, while at the QC level 2 (mean value 0.75 μ mol/l) the between-day precision was 5.5%. The results demonstrated satisfactory assay precision as shown by the % CV values of <15% for the two QC concentration levels.

Recovery: We tested extraction recovery of the drug by spiking the untreated mouse serum pool with metformin at two concentrations (0.2 and 2.0 μ mol/l) using three replicates for each concentration. The percent recovery was determined by comparing the measured concentration with the expected concentration. The analyte was successfully extracted with average recovery of 101.8 %.



Results

Metformin levels measured in treated Pkd1 mutant mice:

We measured serum metformin levels by LC-MS/MS from the individual metformin-treated (300 mg/kg/day in drinking water) mutant mice at around 11 weeks of age after at least one month of metformin treatment (n=20) and at the time of sacrifice (n=19); their mean serum metformin levels were 14.6 (90% CI: $18\cdot6-21\cdot4$) and 17.2 (90% CI: $14\cdot1-20\cdot3$) μ M, respectively. There was a weak direct correlation between serum metformin levels and cystic disease severity (2KW/BW) after one month of treatment (n=20; $r^2=0.16$; p=0.086) and a significant and stronger correlation at the time of sacrifice (n=19; $r^2=0.40$; p=0.0035). The latter association may be due to the fact that metformin is excreted by the kidneys and its drug levels accumulate with moderate to severe kidney failure. Although the four metformin-treated mice with the lowest 2KW/BW (or cystic index) displayed similar gene expression pattern as the salsalate-treated mice (Figure S6), they in fact had the lowest serum metformin levels. These data did not support the notion that the mild disease seen in these mice was due to a variable treatment effect related to serum metformin levels.

Metformin levels measured in patients with ADPKD

| ID# | Disease | Age (yrs) | Gender (M/F) | Metformin Dose | Daily dose of Metformin | [Metformin] (µM) by LC-MS/MS |
|------|---------|--------------|-----------------|--------------------|----------------------------|---------------------------------|
| 8502 | ADPKD | 53 | М | 0.5 g thrice daily | 1·5 g | 1.34 |
| 8602 | ADPKD | 56 | F | 1 g twice daily | 2·0 g | 9.77 |
| 8618 | ADPKD | 46 | М | 1 g twice daily | 2·0 g | 18.8 |
| 8624 | CKD | 68 | М | negative control | 0 | < 0.05 |
| 8638 | ADPKD | 28 | М | 1 g twice daily | 2·0 g | 13.1 |
| 8694 | ADPKD | 31 | F | 1 g twice daily | 2·0 g | 3.80 |

Median [Metformin] (range) based on 5 patients: 9.8 (1.34 to 18.8) μΜ

Conclusion

The mean/median serum metformin concentrations in the treated mutant mice and patients were within the clinical therapeutic range reported in the literature¹⁻³.

Measurement of AMPK Activities

We attempted but failed to directly show activation of AMPK (i.e. phosphorylated AMPK (pAMPK) and phosphorylated acetyl-CoA carboxylase (pACC)) in the *Pkd1* mutant kidneys by salicylate treatment. However, there were a number of confounders which we believe render the interpretations of these results unreliable.

AMPK comprised a heterotrimeric complex consisting of a catalytic α subunit and regulatory β and γ subunits, and exists in multiple isoforms ($\alpha 1/\alpha 2$, $\beta 1/\beta 2$, $\gamma 1/\gamma 2/\gamma 3$) encoded by different genes (PRKAA1/2, PRKAB1/2, PRKAG1/2/3). In normal mouse kidney, both $\alpha 1$ & $\alpha 2$ isoforms of AMPK are expressed, with a greater extent of $\alpha 2$ than $\alpha 1$ at a ratio of 3 to 2; AMPK $\beta 1$ is the predominant isoform in normal adult rodent and human kidneys^{1,3}. In addition, microarray and RNAseq analysis show stronger mRNA expression of PRKAA2, PRKAB1 and PRKAG1 (encoding AMPK $\alpha 2$, $\beta 1$ and $\gamma 1$) in the normal mouse and human kidneys^{3,4} suggesting AMPK $\alpha 2/\beta 1/\gamma 1$ is the predominant isoform in normal adult kidney. However, little is known about the differences in expression of AMPK subunits between different cell types within the kidney.

There is also evidence for distinct functions of different AMPK isoforms in kidney. In renal fibrosis, AMPK α1 plays a deleterious role, while AMPK α2 plays a protective role. Unilateral ureteral obstruction (UUO) or ischemia-reperfusion injury (IRI) induces the isoform shift from AMPK α2 towards α1, which participates in the development of renal fibrosis^{5,6}. Targeted disruption of AMPK α1 inhibits fibroblast activation and attenuates renal fibrosis⁶. On the other hand, AMPK α2 deficiency enhanced EMT, fibrosis and inflammation in mouse UUO kidneys and AMPK α2 expression reduces renal EMT and inflammation after injury through interaction with $CK2\beta^7$. Metformin attenuates renal fibrosis in both AMPK α 2-dependent and independent manners8. Fibrosis and inflammation are common findings in ADPKD. Consistent with the isoform shift from AMPK $\alpha 2$ towards $\alpha 1$ in renal fibrosis, we found in our microarray study an increased expression of *Prkaa1* (1.2-fold vs WT, FDR p-value = 0.01) and a decreased expression of Prkaa2 (-1.3-fold vs WT, FDR p-value = 7.90E-05) in Pkd1 mutant kidneys; and salsalate treatment significantly increased the expression of Prkaa2 (1.2-fold vs KO, FDR p-value = 0.02) (Figure 2). In addition, we previously performed global gene profiling on cysts of different size vs. minimally cystic tissue (MCT) from human PKD1 polycystic kidneys⁵. At the mRNA level, we also found an increased expression of PRKAA1 (1.5-fold vs MCT, FDR p-value = 0.0005) in human PKD1 renal cysts, although no significant change in the expression of PRKAA2.

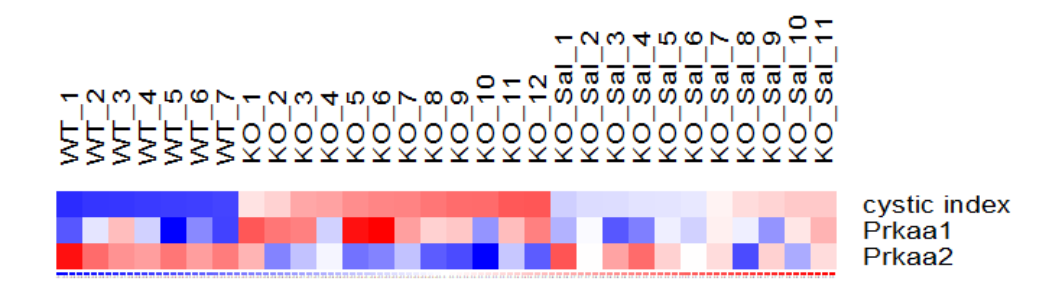
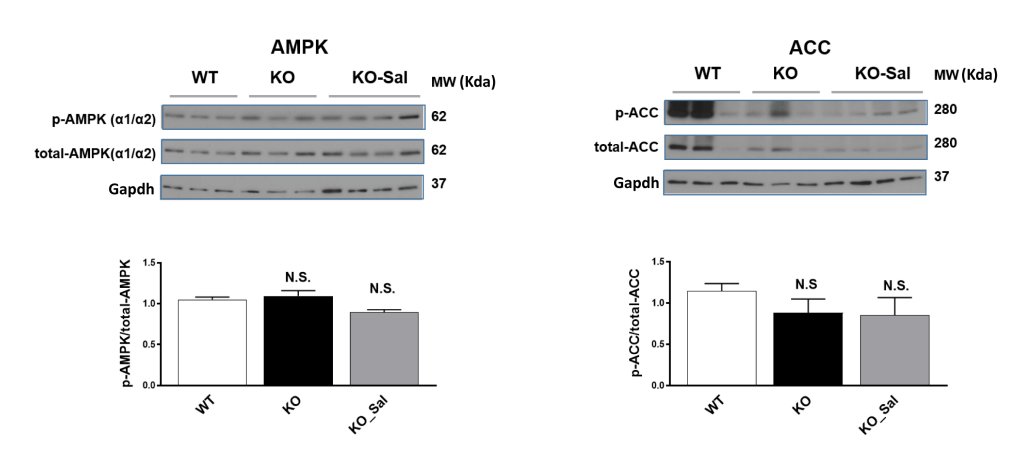


Figure 2: Gene expression profiling showing up-regulation of Prkaa1 and down-regulation of Prkaa2, consistent with isoform shift from Ampk $\alpha 2$ towards $\alpha 1$ in mutant (compared to WT) Pkd1 kidneys; salsalate treatment significantly increased the expression of Prkaa2. Each column represents a sample and each row, a gene. Red colour indicates greater while blue colour indicates less than the mean (white colour) expression value.

Given the protective role of AMPK $\alpha 2$ and deleterious role AMPK $\alpha 1$ in kidney, we hypothesized that salsalate (salicylate) might only activate AMPK $\alpha 2$ through direct interaction with AMPK $\beta 1$ in PKD. However, we could not detect any difference in AMPK and ACC protein levels between salsalate and other groups by Western blot:



However, detection of changes in pAMPK and its target protein pACC is technically challenging. First, the antibodies (anti-pAMPK, anti-AMPK, anti-pACC, anti-ACC) we used in this study did not allow us to differentiate between the different isoforms (the sequences around Thr172 are identical in AMPK $\alpha 1$ and $\alpha 2$, and the anti-pT172 antibody does not distinguish the two AMPK catalytic subunits). Second, considering AMPK is a metabolic sensor, AMPK phosphorylation is very sensitive to rapid changes in metabolites during sacrifice. Freeze-clamping of tissue *in situ* is generally applied to stabilize pAMPK and pACC levels during tissue collection for study of AMPK activity. In our protocol, we euthanized all the mice by cervical dislocation, then collected and weighted the kidneys before snap freezing. Thus, the tissue retrieval procedure might have inadvertently activated both

pAMPK and pACC, such that the observed changes might not reflect the real biological changes. Finally, AMPK complexes containing the different isoforms may exist in different cell types or different subcellular locations. Using the whole kidney lysate, we may not able to detect the differences by Western blot.

- Lieberthal W, Zhang L, Patel VA, Levine JS. AMPK protects proximal tubular cells from stress-induced apoptosis by an ATP-independent mechanism: potential role of Akt activation. Am J Physiol Renal Physiol 2011; 301(6): F1177-92.
- 2. Salatto CT, Miller RA, Cameron KO, et al. Selective Activation of AMPK β1-Containing Isoforms Improves Kidney Function in a Rat Model of Diabetic Nephropathy. *J Pharmacol Exp Ther* 2017; **361**(2): 303-11.
- 3. Brunskill EW, Park JS, Chung E, Chen F, Magella B, Potter SS. Single cell dissection of early kidney development: multilineage priming. *Development* 2014; **141**(15): 3093-101.
- Song X, Di Giovanni V, He N, et al. Systems biology of autosomal dominant polycystic kidney disease (ADPKD): computational identification of gene expression pathways and integrated regulatory networks. Hum Mol Genet 2009; 18(13): 2328-43.
- Mia S, Federico G, Feger M, et al. Impact of AMP-Activated Protein Kinase α1 Deficiency on Tissue Injury following Unilateral Ureteral Obstruction. PLoS One 2015; 10(8): e0135235.
- 6. Wang Y, Jia L, Hu Z, Entman ML, Mitch WE. AMP-activated protein kinase/myocardin-related transcription factor-A signaling regulates fibroblast activation and renal fibrosis. *Kidney Int* 2018; **93**(1): 81-94.
- 7. Qiu S, Xiao Z, Piao C, et al. AMPKα2 reduces renal epithelial transdifferentiation and inflammation after injury through interaction with CK2β. *J Pathol* 2015; **237**(3): 330-42.
- 8. Feng Y, Wang S, Zhang Y, Xiao H. Metformin attenuates renal fibrosis in both AMPKα2-dependent and independent manners. *Clin Exp Pharmacol Physiol* 2017; **44**(6): 648-55.

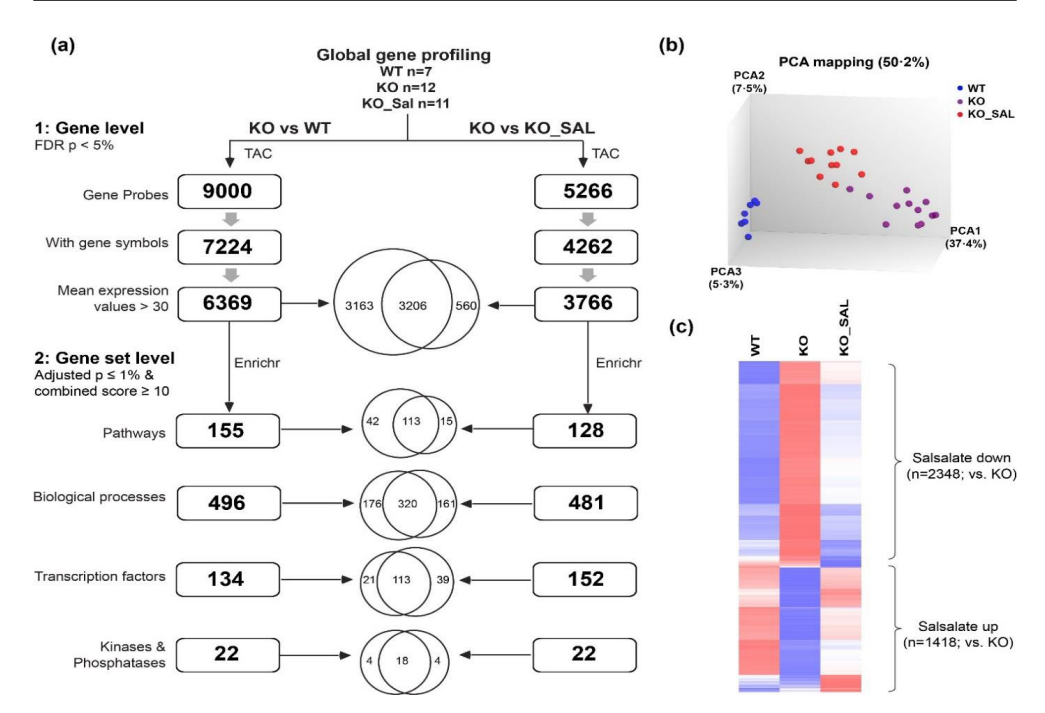


Figure S1: Identification of differentially expressed genes by Transcriptome Analysis Console (TAC) and gene set enrichment by Enrichr

(a) Filtering steps applied to identify differentially expressed genes (DEGs) for gene set enrichment analysis (GSEA). Venn diagram showing overlapping and non-overlapping genes and gene sets. Salsalate treatment altered the expression of ~50% of DEGs enriched in *Pkd1* mutant (vs. to WT) kidneys. (b) Principle component analysis (PCA) of normalized expression levels of 10,000 independent transcripts. The first 3 principal components accounted for 50·2% of the explained variance and clustered apart samples from different genotypes and treatment. (c) Hierarchical clustering showing salsalate treatment attenuated changes in the expression levels of most of 3,766 DEGs enriched in *Pkd1* mutant (vs. to WT) kidneys. Columns represent 3 groups (WT, KO and KO_SAL) and rows represent the mean expression values of each group for each gene; red indicates greater than the mean (white) and blue, less than the mean values. Wild type (WT); *Pkd1* knock-out (KO), and *Pkd1* KO mice treated by Salsalate (KO_SAL).Note: PCA was used to identify key variables in a multidimensional data set that explain the differences in the observations. PCA on probe intensity data identified 3 components (i.e. PCA1, PCA2, PCA3) that account for mostof the variability among the studied samples. Samples that are close together in the plot have similar expression intensities, and samples that are far apart in the plot have dissimilar expression intensities.

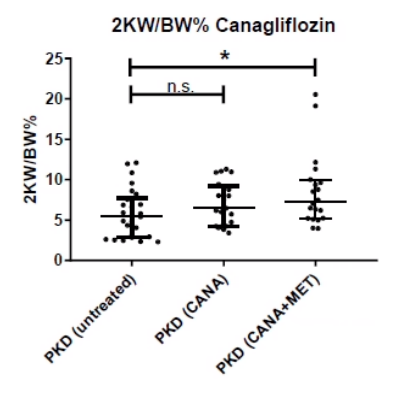


Figure S2: Canagliflozin treatment did not slow PKD Neither Canagliflozin alone (CANA) nor Canagliflozin+Metformin (CANA+MET) reduced the 2KW/BW%. CANA+MET was associated with higher 2KW/BW% compared to untreated mutant control mice (One-way ANOVA followed by Dunnett's test for multiple comparison post-hoc, *P < 0.05).

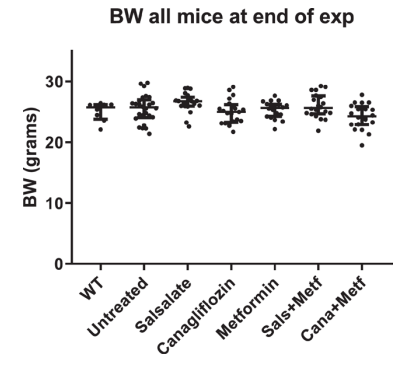


Figure S3: Body weight of all mice at the end of the study

There was no difference in body weight (BW) between mice across different experimental groups at the end of the study (one-way ANOVA, p>0.05 corrected for multiple testing).

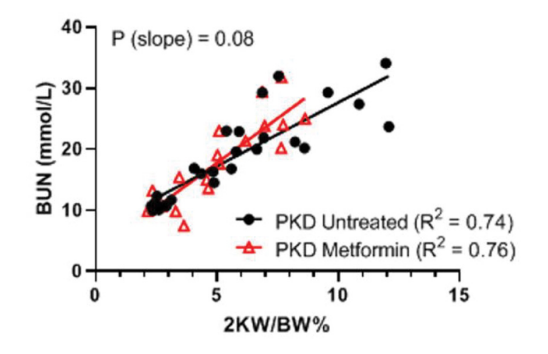


Figure S4: Correlation of blood urea nitrogen to 2KW/BW There was a strong correlation between BUN (mmol/L) at the time of sacrifice and 2KW/BW% in both the metformintreated (R²=0.76) and untreated control (R²=0.74) mutant *Pkd1* mice. The slope of this correlation in the metformintreated mice tended to be slightly steeper; however, this was not statistically significant (P = 0.08).

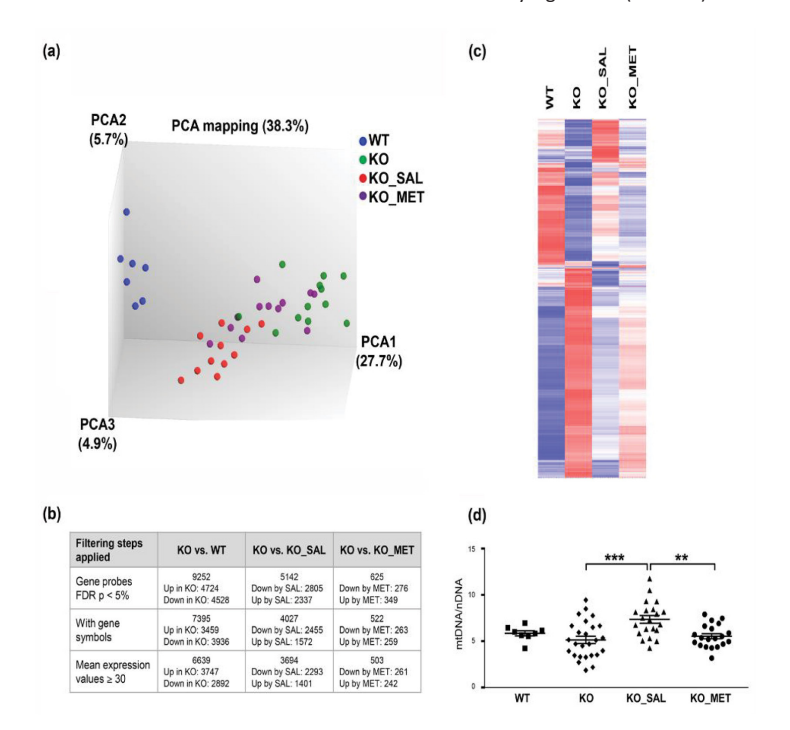


Figure S5: Global gene expression and mtDNA/nDNA ratio in metformin-treated mutant (KO_MET) mice compared to untreated (KO) and salsalate-treated (SAL_KO) mutant mice

As a quality control measure, we assessed metformin treatment on global gene expression. By Principal Component Analysis (PCA; panel a), most samples from the KO_MET mice clustered with samples from the KO mice although 4 KO_MET samples did overlap with the SAL_KO mice. There were fewer (625 vs. 5142; ~1/9) differentially expressed genes between the KO_MET and KO mice as compared to KO_SAL vs KO mice (panel b). Both the global gene expression pattern (panel c) and mtDNA/nDNA (panel d) of the KO_MET samples closely resembled the KO samples. Overall, these findings are consistent with a lack of effect with metformin treatment in this study.

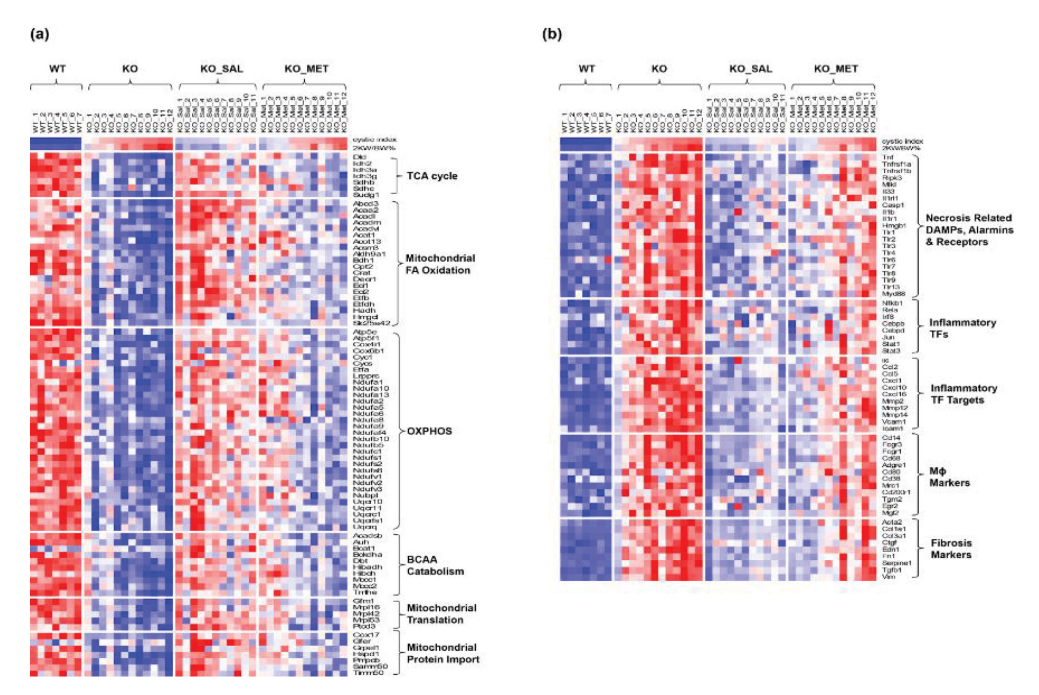


Figure S6. Expression pattern of genes regulating (a) metabolism and (b) innate immunity in metformin-treated mutant (KO_MET) mice compared to untreated (KO) and salsalate-treated (SAL_KO) mutant mice

Of interest, the four samples (KO_Met_1-4) from the KO_MET mice that clustered with the KO_SAL mice had the mildest cystic disease of the group and showed a high concordance of expression patterns of genes that regulate metabolism and innate immunity. However, it is unclear whether the finding was related to variable treatment effect from different metformin kidney tissue levels or reflect that of a phenotypic bias (i.e. gene expression pattern associated with mild disease).

Table S1. Top-ranked inhibited and activated transcriptional factors enriched in *Pkd1* mutant mouse kidneys but attenuated by salsalate treatment as predicted by Enrichr

| Top-ranked inhibited transcription factors (TFs) enriched in <i>Pkd1</i> mutant mouse kidneys but attenuated by salsalate treatment | Top-ranked inhib- ited TFs enriched in <i>Pkd1</i> mutant (vs. WT) mice | | Top-ranked activated TFs in salsalate-treated (vs. untreated) <i>Pkd1</i> mutant mice | |
|---|--|---------|---|---------|
| | Adjusted P-value | Z-score | Adjusted P-value | Z-score |
| RXR_22158963_ChIP-Seq_LIVER_Mouse | 2·68E-37 | -1.44 | 3·67E-23 | -1·44 |
| PPARA_22158963_ChIP-Seq_LIVER_Mouse | 6·39E-35 | -1.48 | 2·34E-21 | -1·48 |
| LXR_22158963_ChIP-Seq_LIVER_Mouse | 2·77E-21 | -1·41 | 3·06E-14 | -1·41 |
| ESRRB_18555785_ChIP-Seq_MESCs_Mouse | 8·71E-22 | -2.03 | 4·90E-12 | -2.02 |
| ESR1_17901129_ChIP-ChIP_LIVER_Mouse | 1·20E-13 | -2.78 | 1·55E-08 | -2.78 |

Table S1 (continued)

| Top-ranked activated TFs enriched in <i>Pkd1</i> mutant mouse kidneys but attenuated by salsalate treatment | Top-ranked activated TFs enriched in <i>Pkd1</i> mutant (vs. WT) mice | | Top-ranked inhib- ited TFs in sal- salate-treated (vs. untreated) Pkd1 mutant mice | |
|---|---|---------|--|---------|
| | Adjusted P-value | Z-score | Adjusted P-value | Z-score |
| IRF8_27001747_Chip-Seq_BMDM_Mouse | 4·63E-43 | -1.50 | 7·19E-39 | -1.50 |
| NCOR_22465074_ChIP-Seq_MACROPHAGES_Mouse | 2·66E-34 | -1·47 | 1·37E-36 | -1·48 |
| SMRT_22465074_ChIP-Seq_MACROPHAGES_Mouse | 2·40E-32 | -1·46 | 5·74E-35 | -1·47 |
| RELA_24523406_ChIP-Seq_FIBROSARCOMA_Human | 1·63E-29 | -1.71 | 6·00E-35 | -1.72 |
| NUCKS1_24931609_ChIP-Seq_HEPATOCYTES_Mouse | 1·56E-36 | -2·27 | 1·25E-33 | -2·25 |
| RUNX2_24764292_ChIP-Seq_MC3T3_Mouse | 3·75E-24 | -1·47 | 1·88E-31 | -1·48 |
| MECOM_23826213_ChIP-Seq_KASUMI_Mouse | 2·54E-28 | -1·49 | 2·90E-30 | -1·49 |
| MYB_21317192_ChIP-Seq_ERMYB_Mouse | 4·12E-19 | -1.99 | 8·28E-30 | -2.01 |
| CEBPB_21427703_ChIP-Seq_3T3-L1_Mouse | 1·22E-14 | -1·40 | 5·64E-29 | -1·44 |
| CEBPD_21427703_ChIP-Seq_3T3-L1_Mouse | 3·56E-22 | -1.53 | 1·72E-25 | -1.53 |

The Geneset library ChEA was used for the above analysis.

Supplementary References

- Lantinga-van Leeuwen IS, Leonhard WN, van der Wal A, Breuning MH, de Heer E, Peters DJ. Kidney-specific inactivation of the Pkd1 gene induces rapid cyst formation in developing kidneys and a slow onset of disease in adult mice. *Hum Mol Genet* 2007; 16(24): 3188-96.
- Chandel NS, Avizonis D, Reczek CR, et al. Are metformin doses used in murine cancer models clinically relevant? Cell Metab 2016; 23(4): 569-70.
- 3. He L, Wondisford FE. Metformin action: concentrations matter. Cell Metab 2015; 21(2): 159-62.
- 4. Fleischman A, Shoelson SE, Bernier R, Goldfine AB. Salsalate improves glycemia and inflammatory parameters in obese young adults. *Diabetes Care* 2008; **31**(2): 289-94.
- Smith BK, Ford RJ, Desjardins EM, et al. Salsalate (salicylate) uncouples mitochondria, improves glucose homeostasis, and reduces liver lipids independent of AMPK-β1. Diabetes 2016; 65(11): 3352-61.
- Kuleshov MV, Jones MR, Rouillard AD, et al. Enrichr: a comprehensive gene set enrichment analysis web server 2016 update. Nucleic Acids Res 2016; 44(W1): W90-7.
- Mottillo EP, Desjardins EM, Crane JD, et al. Lack of adipocyte AMPK exacerbates insulin resistance and hepatic steatosis through brown and beige adipose tissue function. Cell Metab 2016; 24(1): 118-29.
- 8. Lian X, Wu X, Li Z, et al. The combination of metformin and 2-deoxyglucose significantly inhibits cyst formation in miniature pigs with polycystic kidney disease. *Br J Pharmacol* 2019; **176**(5): 711-24.
- U.S. Department of Health and Human Services, Food and Drug Administration, Center for Drug Evaluation
 and Research. Guidance for industry: estimating the maximum safe starting dose in initial clinical trials for
 therapeutics in adult healthy volunteers. July 2005.